RIPARIAN AND GEOMORPHIC DISTURBANCE FROM A HIGH-MAGNITUDE FLOOD ON THE BLANCO RIVER IN THE TEXAS HILL COUNTRY

by

John Nicholas Phillips

A thesis submitted to the Graduate Council of
Texas State University in partial fulfillment
of the requirements for the degree of
Master of Science
with a Major in Geography
May 2017

Committee Members:

Dr. Kimberly Meitzen, Chair

Dr. Jason Julian

Dr. Edwin Chow

FAIR USE AND AUTHOR'S PERMISSION STATEMENT

Fair Use

Duplication Permission

DEDICATION

First and foremost, I would like to thank my fiancé Rachel. Thank you for putting up with me when I was stressed and stuck at the computer for hours and days at a time. I promise I will return the sandwiches and backrubs when you are writing your thesis. Thank you to my mother Laura for always believing in me and pushing me to do my best. Thank you for always being there to listen and encourage me. Tia, I would not have the love for learning that I do if you would not have read to me when I was young. Thank you for always being a steward of my education and success. Perry, thank you for helping me manage life and for always being there to answer my 'how do I fix this' questions. I hope I can be half the man you are one day. Robin, thank you for being a beacon of love and always having the best advice for Rachel and me. Tim, Brandon, Greyson, and Melissa, you are the best siblings anyone could ask for and I love you. I am dedicating this thesis you, our family, and my new family with Rachel. Thank you for making life great.

ACKNOWLEDGEMENTS

This paper would not have been possible without the guidance and patience of the professors of the Texas State Geography Department. First, I would like to thank Dr. Meitzen for helping me form this project after the many struggles I faced in its initial iterations. Thank you for everything you've taught me, your understanding of my work commitments, pushing me to improve my data, and being an overall great advisor. I would also like to thank Dr. Julian for teaching a great water resources class and hosting the water reading group with Dr. Meitzen. Having not taken a water class in my undergraduate studies, you both instilled a great interest in the subject for me. I admire both of your work and hope to work at a water-related job in the future. I would like to thank Dr. Chow as well for teaching me Python programming and how to approach problem solving in GIS. The skills you have taught me have already opened job opportunities and helped me to fulfill myself as a geographer. Finally, I would like to thank are Mark Carter for showing me the Environmental Service Committee and helping me get my first internship and job offer.

TABLE OF CONTENTS

Page

ACKNOWLEDGEMENTS v

LIST OF TABLES viii

LIST OF FIGURES x

ABSTRACT xii

CHAPTER

I. INTRODUCTION 1

II. LITERATURE REVIEW 3

a. Floodplain development theories 3
b. Types of floodplain stripping 5
c. Bio-hydro-geomorphic Disturbance and Recovery 6
d. Research significance 8

III. METHODS 10

a. Study Area: Geology and Biogeography 10
b. Study Area: Land Use 12
c. Data 12
d. Disturbance mapping 18
e. Disturbance calculation 26
f. Analysis methods 26
g. Hydrologic and hydraulic analysis 31

IV. RESULTS 33

a. River statistics 33
b. Riparian disturbance: Area totals 36
c. Geomorphic disturbance: Area totals 39
d. Riparian and geomorphic disturbance intersection 42
e. River statistics and disturbance correlation 48
f. Relative disturbance 54

V. DISSCUSSION 60

a. River measurements and calculations 60
b. Disturbance area totals 64
c. Riparian and geomorphic disturbance intersections 69
d. Floodplain Stripping, Meanders, and Other Disturbance Forms 70
e. Tributary confluences 74
f. Disturbance statistics: Absolute vs relative 79
g. Digitizing and Sampling Caveats 80
h. Future studies 82

VI. CONCLUSION 88

APPENDIX SECTION 89

LITERATURE CITED 93

LIST OF TABLES

Table **Page**

1. Correlation Coefficients and Their Interpretations 33

2. Descriptive Statistics for the River in the Study Area Extent and Calculated Channel Net Gain and Net Loss 34

3. Pearson Correlation of River Measurements and Calculations Taken Along the River in Relation to Each Other 35

4. Riparian Disturbance Category Totals 38

5. Riparian Disturbance per Category Relative to Total Disturbance in that Category 38

6. Geomorphic Disturbance Category Totals 41

7. Geomorphic Disturbance Relative to Total Disturbance 41

8. Disturbance Intersection: Riparian and Geomorphic 45

9. Relative Intersection Area: Riparian and Geomorphic 45

10. Pearson Correlation of Total Area per Sample Circle between Disturbance Categories 46

11. Spearman's Rho Correlation of Total Area per Sample Circle between Disturbance Categories 47

12. River Statistics, Stream Power, and Riparian Disturbance Pearson Correlation 50

13. River Statistics, Stream Power, and Riparian Disturbance Spearman's Rho Correlation 51

14. River Statistics, Stream Power, and Geomorphic Disturbance Pearson Correlation 52

15. River Statistics, Stream Power, and Geomorphic Disturbance Spearman's Rho Correlation 53

16. Relative Riparian Disturbance Pearson Correlations..... 56

17. Relative Riparian Disturbance Spearman's Rho Correlations..... 57

18. Relative Geomorphic Disturbance Pearson Correlations 58

19. Relative Geomorphic Disturbance Spearman's Rho Correlations..... 59

LIST OF FIGURES

Figure **Page**

1. Discharge at the USGS Blanco River near Kyle Stream Gage 1

2. The Blanco River Drainage Basin in Central Texas 14

3. Extents of Available Imagery 15

4. Riparian Disturbance Categories 20

5. Geomorphic Disturbance Categories 23

6. Disturbance Categorization Example 25

7. Longitudinal Profile of the Blanco River Study Area 29

8. Sample Circle Illustration 31

9. Channel Width versus Floodplain Width 63

10. Disturbance Category by FEMA Floodplain 64

11. Pre-Flood Disturbance Gradient Example 66

12. Post-Flood Disturbance Gradient Example 67

13. Post-Flood Disturbance Gradient Example Mapped and Categorized 68

14. Across Meander Scour 73

15. Deposition at Lone Man Creek 75

16. Lone Man Creek Confluence 76

17. Cypress Creek Confluence 77

18. Halifax Creek Confluence 78

19. The Blanco River Pre-October Flood 84

20. The Blanco River Post-October Flood 85

21. The Blanco River Pre-Memorial Day Flood 86

22. The Blanco River Post-Memorial Day Flood 87

ABSTRACT

Rivers of the Central Texas Hill Country are subject to significant bio-geomorphologic changes along the riparian corridor during low-frequency, high-magnitude catastrophic flood events. One significant change can involve floodplain stripping, which is the removal of alluvium and vegetation along the riparian corridor. Discharge magnitude, valley morphology, vegetation, and land cover can influence floodplain stripping processes. The Blanco River in Central Texas is an ideal system to study flood disturbances, which can include the process of floodplain stripping. The upper reaches of the river drain the high relief Hill Country landscape of the Edwards Plateau where the main stem channel is laterally confined by limestone bedrock, steep canyons, and thin soils. The lower reaches of the river transition across the Balcones Escarpment to a lower relief valley with deeper soils and a wide floodplain as it nears its confluence with the San Marcos River in the Coastal Plain. In May 2015, the Blanco River experienced catastrophic flooding with estimates of 33 cm of precipitation falling in its headwaters over only a few hours. Imagery from pre- and post-flooding was used to identify and categorize the various patterns of disturbance along the river that range from complete floodplain stripping to minimal disturbance. A custom method was developed to sample disturbance along the river. Relationships between total disturbance area, disturbance area per floodplain, and disturbance area per sample were examined. Results show the most severe disturbance occurred within the floodway near the channel and decreased with distance. Patterns of biogeomorphic disturbance mentioned in previous literature such as across meander scour and parallel chute scour were identified as well as patterns of severe disturbance at tributary confluences.

I. INTRODUCTION

The concept of 'floodplain stripping' was introduced by G. C. Nanson (1986) and is described as a process that occurs when accumulated alluvium and riparian vegetation are removed from the floodplain during high magnitude flood events. The Blanco River is susceptible to flash flooding when large volumes of overland runoff accumulate over a short period of time. Factors such as the increase of impervious cover due to rapid urbanization and the removal of vegetation along the riparian corridor for easy river access have increased vulnerability to flash flooding (Baker 1977).

On May 25, 2015, Central Texas experienced a series of large thunderstorms which brought over 33 centimeters of rain to the headwaters of the Blanco River watershed over the period of only a few hours. This event led to near record-setting catastrophic flooding of the Blanco and San Marcos Rivers. As shown in Figure 1,

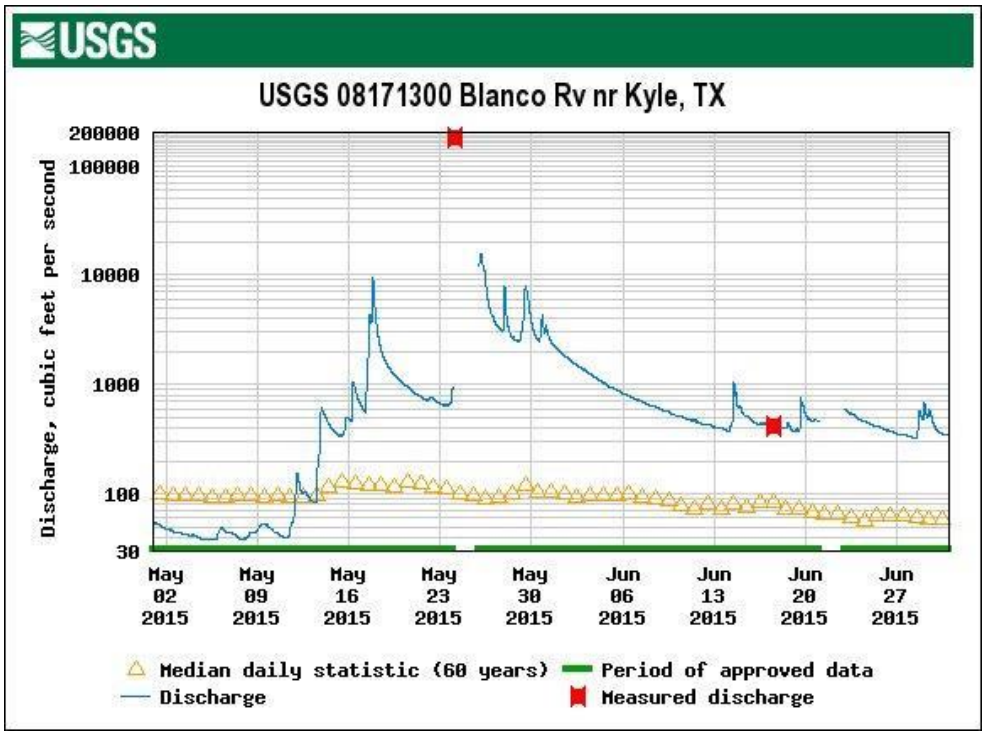

Figure 1 Discharge at the USGS Blanco River near Kyle gage for May 2,2015 to June 27, 2015 in cubic feet per second

discharge estimates for the flood at the Blanco River near Kyle USGS gage range from 175,000-180,000 f^3s^{-1} (USGS 08171300, NWIS 2016).

This study used a combination of satellite and aerial imagery integrated within a Geographic Information System (GIS) to identify and map patterns of disturbance along the main stem Blanco River. Valley controls were examined along various sections of the river corridor to compare riparian disturbance response of different reaches.

Overall, this study seeks to address the following questions:

1. What are some of the biogeomorphic disturbances and their spatial coverage from the catastrophic flooding on the riparian corridor of the Blanco River?
2. How do valley physiographic controls, such as floodway width, channel width, and specific stream power contribute to varied patterns of flood disturbance on the Blanco River riparian corridor?

II. LITERATURE REVIEW

a. Floodplain development theories

Traditional floodplain development theories attribute floodplain deposits to lateral and vertical accretion which occur during bankfull and overbank flow, respectively. According to Wolman and Leopold (1957), overbank deposition occurs on both small tributaries and large rivers gradually forming floodplains until the river becomes increasingly channelized within the its valley and eventually develops a new floodplain; abandoning the older surface as a terrace. Over extended time periods (hundreds to thousands of years) and driven by frequent, moderate-scale events, this process will continue within the valley as the river adjusts to gradient and base level changes Wolman and Miller (1960).

Although Wolman and Miller (1960) have shown that the majority of river and floodplain modifications take place during frequent, moderate flood events, Baker (1977) shows that stream-channel responses can vary widely under different climatic and physiographic conditions, including those characteristic of Central Texas. The Wolman-Miller model accurately characterizes stream-channel responses for perennial rivers in the central United States which drain low-relief landscapes characterized by thick soils, that have infiltration rates that exceed normal precipitation rates, and low runoff. However, in Central Texas, many of the streams are seasonally intermittent or ephemeral and they drain steep-relief landscapes, covered with thin-clayey soils and resistant limestone bedrock, and high overland flow. In this setting, these processes when coupled with localized, intense, and long duration precipitation events can lead to catastrophic flash flooding with high magnitude stream discharges that rise and fall quickly. In Australia,

similar flash-flood conditions mobilized and transported floodplain sediments (2metersdeep and 30meterswide) more than 500 meters downstream in the Clyde and Manning Rivers of New South Wales, Australia (Nanson 1986).

Due to the variability in physiographic valley and runoff conditions, various classifications exist for stream and floodplain responses to discharge and sediment characteristics. Schumm (1963) and Schumm (1968) classify channels by three types, stable, eroding, or accreting, depending on the discharge and sediment load. Nanson and Croke (1992) classify floodplains into three classes, high-energy non-cohesive, medium-energy non-cohesive, and low-energy cohesive relative to stream power and sediment characteristics. These main classes can be further divided by a variety of orders and suborders based on specific floodplain forming processes that involve accretion and erosion, or stripping processes.

Some notable studies on floodplain development and stripping processes in semi-arid regions have been performed on the Clyde and Manning Rivers in Southeast Australia (Nanson and Young 1981, Nanson 1986, Warner 1997) which, like the Blanco River, are characterized by a semi-arid climate with long periods of drought and variable physiography ranging from confined reaches to areas with broad floodplains. The primary climatic difference between Central Texas rivers and the rivers studied in Australia involves temporal rainfall distribution. Southeast Australia experiences a cyclic shift between flood dominated periods and drought dominated periods (Warner 1997). Warner (1997) compared the flood dominated and drought dominated periods and found that higher discharges and more frequent flooding occurs during flood dominated periods, and lower discharges and infrequent flooding occurs during drought periods, and both

flood and drought periods have distinct morphological effects on the Clyde and Manning Rivers. Central Texas differs from the Southeast Australian rivers in that, even during prolonged periods of drought, the region can experience intense rainfall in localized parts of a river basin that produce catastrophic flooding and morphologic change over the period of hours to days. Although distinct climatic factors influence Southeast Australia and Central Texas, their flooding impacts on longitudinally connected stream conditions can result in similar floodplain disturbances including floodplain stripping.

b. Types of Floodplain Stripping

Floodplain stripping is complex and influenced by a variety of factors including river morphology, valley and channel geometry, riparian vegetation, and sediment characteristics. However, similar patterns of stripping have been identified in previous studies. Warner (1997) describes three types of stripping: across meander chutes, parallel chute, and convex bank erosion. Across meander chutes are formed by high flows which cut across a meander and excavate a channel or portions of the floodplain. Chutes can range from low-level chutes which cut to the basal gravels, to high-level chutes where grasses or other cover may still be present and small depressions may be cut and filled with sediment and debris. Parallel chutes are carved alongside the main channel during high flows where there is little alluvium present at the meander apex. Convex bank erosion occurs on the inner bank of a meander when the concave bank is composed of bedrock (Warner 1997).

Other destructive floodplain mechanisms include macroturbulent scour and surface channel scour (Bourke 1994). Macroturbulent scour occurs when vortices form around obstacles such as large tree stands or debris dams creating ‘swirl pits’ on the floodplain.

Surface channel scour forms when confined back channels along the floodplain are excavated by overbank flow during flooding (Bourke 1994).

c. Bio-hydro-geomorphic Disturbance and Recovery

River response to and recovery from disturbance depends on many biologic, hydrologic and geologic controls which affect the river's function and each other. These controls include water discharge, bed material load, bed material size, bank material, channel vegetation and valley morphology (Julian et al. 2016). With its confined limestone bedrock valley, the Blanco River differs morphologically from the alluvial streams studied by Julian et al. (2016). The same controlling factors however affect disturbance in the river system.

River discharge driven by precipitation is a main control for disturbance on the Blanco River and varies widely temporally. High intensity flooding with low recurrence intervals have given Central Texas one of the highest Flash Flood Magnitude Index (FFMI) ratings in the country (Baker 1977). FFMI evaluates the magnitudes of regular flood events in comparison to rare severe flood events (Beard 1975). Valley morphology is another major control for disturbance on the Blanco River. In some areas, channel widening, lateral migration, and downcutting are prohibited by the limestone bedrock. However, infrequent catastrophic flooding has been shown to cause significant reworking of floodplain sediments contained by resistant limestone valleys resulting in the erosion of scour holes on the floodplain surface as well as the deposition of gravel bars and mid-channel islands (Patton and Baker 1977).

Vegetation in and along the channel and floodplain is another important control for disturbance. Riparian vegetation has been shown to increase resistance to disturbance by

stabilizing river banks via root reinforcement (Abernethy and Rutherford 2001). The above ground biomass can promote vertical accretion during floods because its resistance reduces flow velocities and suspended sediment entrainment, resulting in increased sedimentation (Meitzen, 2005). Nanson (1986) proposed a disequilibrium model for floodplain development whereby vertical accretion occurs during normal and moderate flood flows. Vegetation establishes in the accumulated deposits until it forms a stable, mature riparian plant community, and then rather abruptly the riparian area is eroded during a single flood event or cluster of low-frequency, high-intensity flood events. This disturbance process, is part of a disequilibrium cycle, that essentially restarts the floodplain accretion processes until the next major disturbance takes place causing the system to once again cross a threshold resetting the riparian development.

The magnitude threshold at which a flood event needs to reach in order to erode a bank is increased over time as riparian vegetation establishes itself. Vegetation has been shown to strengthen hydraulic resistance and bank strength in the channel and along the floodplain with tall and dense vegetation increasing roughness and decreasing the peak discharge of floods, especially less severe ones (Anderson et al. 2006). Well established grasses, which are widespread along the Blanco River, have also been shown to stabilize banks due to their robust root systems. In certain conditions, grasses have been shown to provide more mechanical bank stability and cohesion than mature riparian vegetation (Simon and Collison 2002). In many cases, between major flood events, mid-channel islands and other disturbed areas in or near the channel are colonized by pioneer species including the black willow (*Salix nigra* Marshall*)*, which can handle light sedimentation during normal flows and unstable slopes (Hupp 1992).

Anthropogenic factors should also be considered when studying disturbance. Examples of human influence on the Blanco River include land cover changes such as landscaping for aesthetic purposes or for river access and agriculture which have altered the river from its natural state. The removal of riparian vegetation due to landscaping or flood events can result in bank instability, erosion, and channel widening. Multiple dams are also present along the river which have been shown to have many downstream effects on large rivers such as decreases in discharge, sediment load, elevation, and channel width (Julian et al. 2016; Graf 2006). In addition to channel changes, dams and flow diversions have also been shown to affect the extent, heterogeneity, and composition of riparian species downstream (Caskey et al. 2015; Aguiar et al. 2016).

d. Research Significance

While other studies have examined floodplain stripping during climatically regular flood dominated periods (Warner, 1997) and in small tributary systems (Baker, 1977), a lack of research exists for the floodplain stripping that can occur in large river valleys such as the Blanco River which experience highly variable precipitation events that produce low frequency, high magnitude catastrophic flooding. Additionally, quantifying floodplain stripping processes at the scale of multiple kilometers was not conducted in Warner and Nanson's 1970s and 1980s studies or Baker's 1977 study on Central Texas. High resolution pre- and post- flood imagery allow this study to examine specific patterns of disturbances along 52 km of river and examine factors that influence various patterns of flood disturbance.

Previous studies have used on-screen digitizing techniques to examine geomorphic and hydrologic change. For example, Graf (2006) examined numerous river

reaches to assess the geomorphic differences in regulated and unregulated reaches. Using aerial imagery, Graf (2006) mapped the functional complexity of geomorphic patches at the reach-scale to examine the downstream effects dams. A previous study, Forman and Godron (1981), also examined ecologic patches on the landscape and their relationship with disturbances. The present study is limited to channel and riparian vegetation changes. Understanding these disturbance patterns has implications for public and private riparian area management and flood hazard mitigation efforts. With extreme weather events becoming increasingly common due to climate change (IPCC, 2013), it is important to study the effects of high-intensity flood events. Central Texas receives some of the most intense rainfall in the world and flood hazards in the region are increased due to factors such as topography and land cover changes (Baker 1977). On a broader scale, future researchers and water resources officials will be able to use the techniques and results of this study to plan riparian restoration efforts and assess flood impacts on other rivers.

III. METHODS

a. Study Area: Geology and Biogeography

This study was conducted on the riparian corridor of the Blanco River watershed in Central Texas. The Blanco River's headwaters begin in the Edwards Plateau Balcones Canyonlands ecoregion. Also known as the Hill Country, the area is a karst terrain characterized by rolling, eroded limestone hills and a vast network of underground drainage created by dissolution of limestone substrate. This upper portion of the study area is dominated by soils of the Brackett-Eckrant-Real series including areas of Brackett-Rock outcrop consisting of steep, shallow, calcareous clay loam soils and bedrock with slopes ranging from 8 to 30 percent, Eckrant-Rock outcrop made up of steep, rocky, shallow, clay soils and Comfort complex soils consisting of shallow, stony, clay soils near the channel with slopes ranging from 1 to 8 percent (NRCS 2016). These shallow soils and outcrops of upper Cretaceous limestone, mostly from the Glen Rose formation (TWDB 2017), make up the headwaters of the river as well as the canonized reaches of most of the upper river. The Glen Rose limestone is highly erodible and forms gullies in the upper region of the drainage basin and other karst features throughout (Smith et al. 2015).

The Blanco River is fed by spring flow throughout the drainage basin; however, depending on climate conditions, the main stem and tributaries can be perennial, intermittent, or ephemeral. Surface-groundwater interactions are prevalent along the Blanco River as it interacts with Trinity aquifer units in the upper portions of the river and Edwards aquifer units in the lower river becoming a gaining river in some areas and a losing river in areas with fractures and karst swallets (Smith et al. 2015). Vegetation

along the riparian buffer includes hardwoods such as the bald cypress (*Taxodium distichum* (L.) Rich.), black willow (*Salix nigra* Marshall), and American sycamore (*Platanus occidentalis* L.), as well as native grasses and shrubs. The Blanco River flows approximately 140 kilometers before reaching its confluence with the San Marcos River. Near the IH-35 corridor, along the Balcones Escarpment, here the Blanco River valley transitions to the Floodplains and Low Terraces ecoregion which is part of the Blackland Prairies ecoregion. The dominate soils in this ecoregion are Houston Black, Heiden, and Wilson series which are well drained permeable soils weathered from Cretaceous age (Houston) to Pleistocene age (Wilson) mudstone. As the floodplain widens downstream, Orif soils, which are moist, frequently flooded soils with 0 – 3 percent slope, become more prevalent directly along the channel and its adjacent floodplains. The lower valley contains more extensive floodplain terraces compared to the river's confined upper reaches, and is characterized by similar forest cover and additionally has grasses such as bluestem (*Andropogon gerardii* Vitman) and yellow Indiangrass (*Sorghastrum nutans* (L.) Nash) (Griffith et al, 2008).

The ecotone between these two regions contains a mixture of the aforementioned soils from both the upper and lower reaches as well as Lewisville silty clay and Seawillow clay loam which range from moderately deep to very deep friable clayey soils to deep, fertile loamy clay soils (NRCS 2016). Because the Blanco intersects the Balcones Escarpment, the river becomes influent as it crosses the fractured limestone of the Edwards Aquifer Recharge Zone. The Blanco River's transition from the Balcones Canyonlands to the Northern Blackland Prairie provides a contrast of channel geometries and physiographic conditions making it a prime location to study variability of flood-

related disturbances. A map of the Blanco River drainage basin is provided in Figure 2.

b. Study Area: Land Use

Hays County, where the entirety of the study area lies, was initially inhabited by indigenous native American tribes, and further settled by Spanish explorers in the early 1700s who established outposts and later missions along the fertile land and pristine waters of the Blanco and San Marcos Rivers. The early to mid-1800s saw increased settlement of pioneers and the establishment of Hays County with prairies used as ranges for cattle and valleys for the cultivation of cotton. Ranching and agriculture were the cornerstone to the Hays County economy throughout the rest of the century with corn, barley and other crops proliferating as railroads were established in the area (Dobie 1948). Presently, agricultural land use, including wheat, hay, oats, peaches, and pecans, and ranching of sheep, cattle, goats, and turkey dominate the Upper Blanco watershed where while urban development (right up to the river's banks) dominates the Lower Blanco River near the cities of Wimberley, Kyle, and San Marcos. The Blanco River also is used for fishing, recreation, and public water supply use and its vegetation cover is mostly evergreen forest (42.9%) and grass/herbaceous vegetation (32.2%) (GBRA 2013). An increase in impervious cover has been seen in the urbanized areas throughout the watershed as well as a loss of tree cover mostly replaced by grasses and shrubs. These trends are expected to continue in the future (Sansom et al. 2010).

c. Data

High-resolution aerial and satellite imagery was used for this study to map pre- and post-flood changes. The aerial imagery being used in the present study was granted courtesy of the Texas Google Imagery Service Pilot Project. The Google Imagery Service

project is a collaboration between numerous Texas state agencies including the Texas Department of Transportation, the Texas Water Development Board, and the Texas Natural Resources Information System (TNRIS). Access to the imagery was requested through an educational research MOU between Dr. Meitzen and TNRIS. More information can be found at https://tnris.org/texas-google-imagery.

The aerial imagery is true color and has a spatial resolution of 15.2 centimeters. The project releases new tiles of imagery throughout each year dating back to 2012. For this paper, I used aerial imagery from 10/2/2014, 1/18/2015 for pre-flood, and 7/13/2015 for post-flood. It is important to note for this project that the aerial imagery does not have full-coverage of the entire state for each year. Instead, the imagery service consists of a series of tiles creating an imagery mosaic for each year.

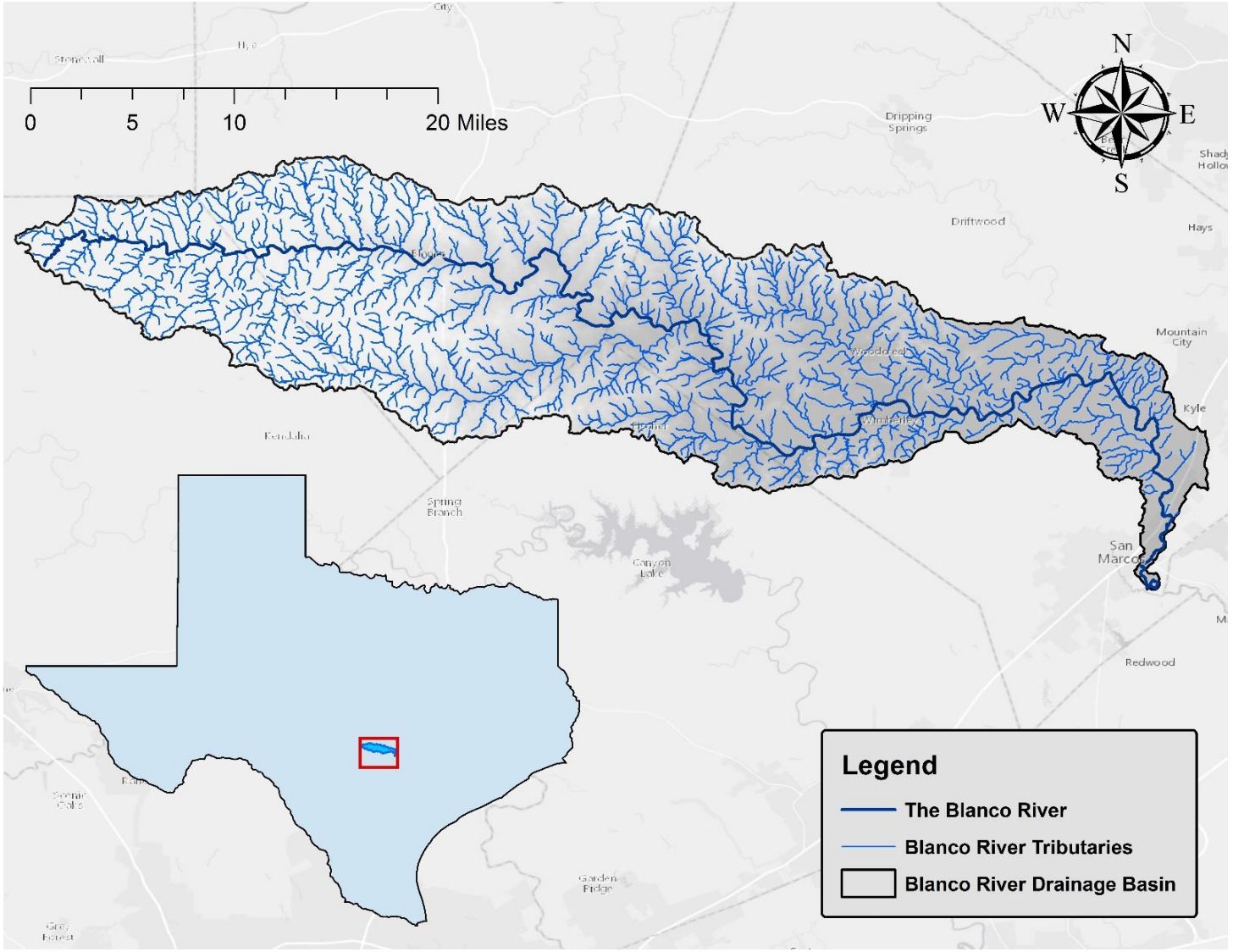

Figure 2 The Blanco River Drainage Basin in Central Texas

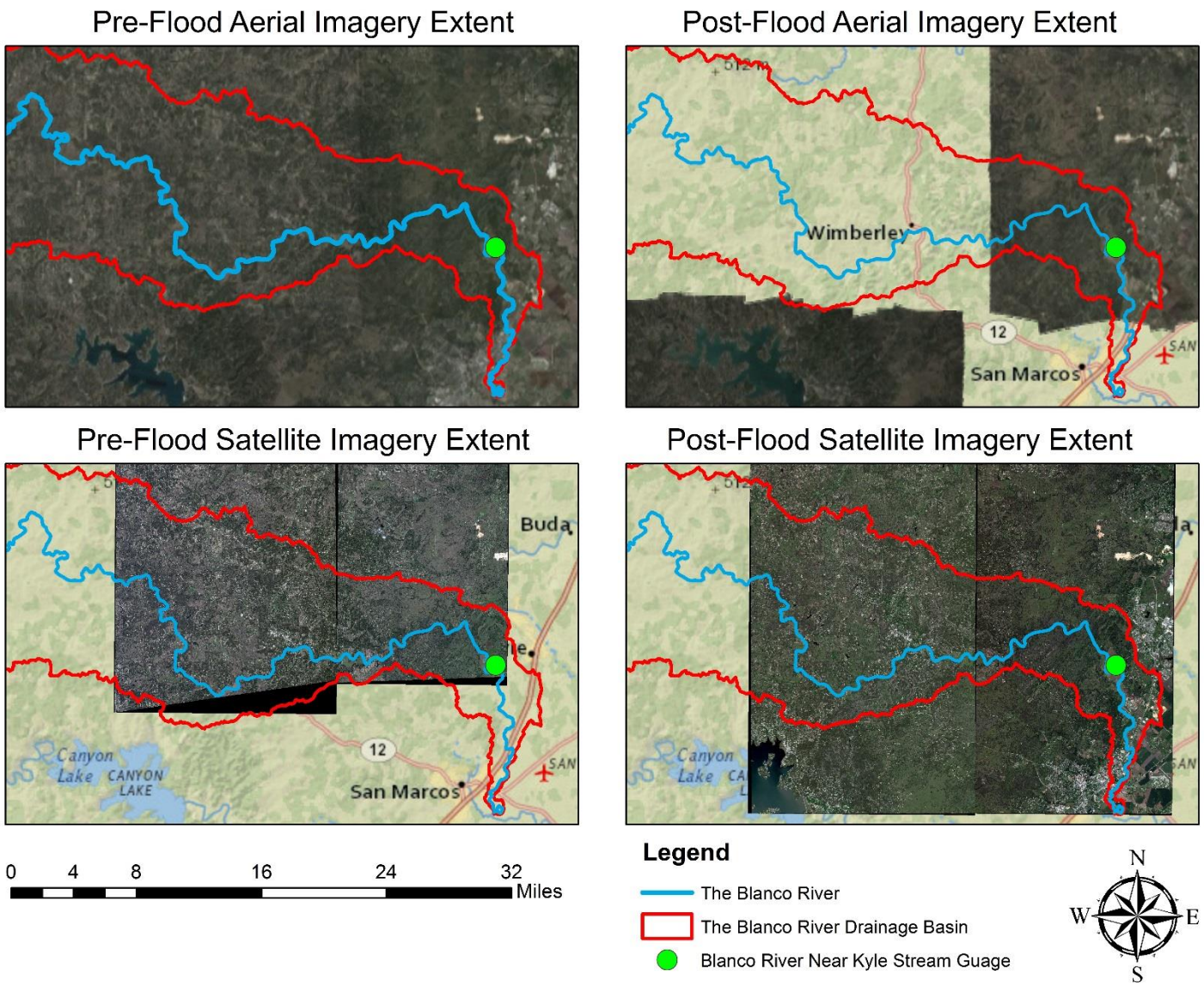

Figure 3 Extents of available imagery. Pre-flood aerial imagery covers the entire drainage basin. The study area is limited by available post-flood imagery.

The high-resolution multispectral satellite imagery used in this study was granted courtesy of the DigitalGlobe Foundation. To acquire Digital Globe imagery, it can be purchased or requested for free (for research purposes) via an application at www.digitalglobefoundation.org/application-process. I requested free use by completing the application process, which included writing a proposal for my study and using the 'ImageFinder' map to locate relevant imagery. Finally, a shapefile of the study area along with specific dates and imagery IDs were provided to Digital Globe.

The DigitalGlobe data I am using includes the WorldView-2 sensor. The WorldView-2 imagery has a spatial resolution of 1.84 meters. The pre-flood satellite imagery was captured on March 14, 2015 and the post-flood imagery date is May 29, 2015.

Although pre-flood aerial imagery covers the entire Blanco River watershed, the extent of the 2015 post-flood aerial imagery ends east of Wimberley and does not cover some areas which were heavily impacted by flooding. The satellite imagery however does cover this area, and while it does not have as fine of a spatial resolution as the aerial imagery, it allows the study area to be extended farther into the western portion of the upper Blanco River watershed.

Because the satellite imagery had a very coarse spatial resolution compared to the aerial imagery, it was difficult to identify disturbance patterns at the target scale of 1:800. To fix this, I created a Python script which pansharpened the WorldView-2 imagery. The script leverages the Create Pansharpened Raster Dataset tool in the arcpy library which fuses datasets with their higher resolution panchromatic raster. This increased the spatial resolution of the imagery from 1.84 meters to the resolution of the panchromatic band which is 0.46 meters. At the new resolution, disturbance patterns could be identified and

categorized at a 1:800 scale. The tool provides various algorithms to choose from including Intensity Saturation Hue (IHS), Brovey, Esri, Gram-Schmidt and Simple Mean. The IHS method was chosen because it sacrifices quality of the underlying spectral values of the imagery for clear, true-color imagery. If spectral indices were being calculated in this study, a different method would have been chosen. The Python script can be found in Appendix A.

The satellite imagery was also slightly misaligned with respect to the aerial imagery due to the sensor being off nadir. To fix this I georeferenced the satellite imagery to match the aerial imagery using houses and other fixed objects along the river as ground control points. Before the imagery could be georeferenced, it had to be projected into the same coordinate system as the Web Map Tile Service (WMTS) aerial imagery. While a more localized coordinate system such as Universal Transverse Mercator (UTM) 14 N would have been preferred for this project, I was unable to project Google's imagery service so I matched all feature classes and imagery in this project to the projection of the Google imagery layers which was WGS 1984 Web Mercator Auxiliary Sphere.

Level II USGS DEMs were used to measure floodplain valley width and slope to estimate the stream power of various reaches. The Level II DEMs were obtained from the United States Geological Survey's 3D Elevation Program (3DEP) and have a resolution of 1/3 arc-second or approximately 10- meters. The data were obtained through The National Map (TNM) Download Viewer at http://viewer.nationalmap.gov/basic. The DEMs were obtained in the form of 4 separate rasters which were then merged in ArcMap and clipped to the Blanco River drainage basin.

Finally, I extracted 100-year and 500-year floodplain layers as well as a floodway layer based on FEMA's National Flood Hazard Layer (NFHL), which is a digital derivation of the Flood Insurance Rate Map (FIRM). The floodplain layers were downloaded from https://www.fema.gov/national-flood-hazard-layer-nfhl in a shapefile format.

d. Disturbance Mapping

Using both the aerial and satellite imagery I mapped (via digitizing) areas of disturbance which occurred along the Blanco River due to the May 2015 flooding. Where it was possible, the aerial imagery was used for digitizing due to it having a finer spatial resolution, however in the upstream sections of the study area, post-flood aerial imagery was not available and instead the satellite imagery was used.

A primary goal of the mapping procedures was to categorize the patterns of disturbance. To accomplish this I created a two-part scheme consisting of attributes that captured both riparian vegetation disturbance and geomorphic disturbance. The riparian vegetation disturbances include five main categories of disturbance and a category for no change (Figure 4). The geomorphic categories include three additional categories. Originally, I created three categories for erosion and three for deposition, however I consolidated the erosion and deposition categories in to three generalized categories labeled geomorphic disturbance and one category for areas of no change (Figure 5). The categories were consolidated because at many areas along the river it is difficult or impossible to distinguish between erosional and depositional features through imagery alone. Additionally, both erosion and deposition may have occurred during the flood event at the areas under scrutiny and labeling the disturbance one or the other involves

too much subjectivity. An illustrated example of the categorization scheme is provided in Figure 6. Over 950 polygons were digitized for riparian disturbance and almost 500 for geomorphic over the 55,000 meters of the river study area.

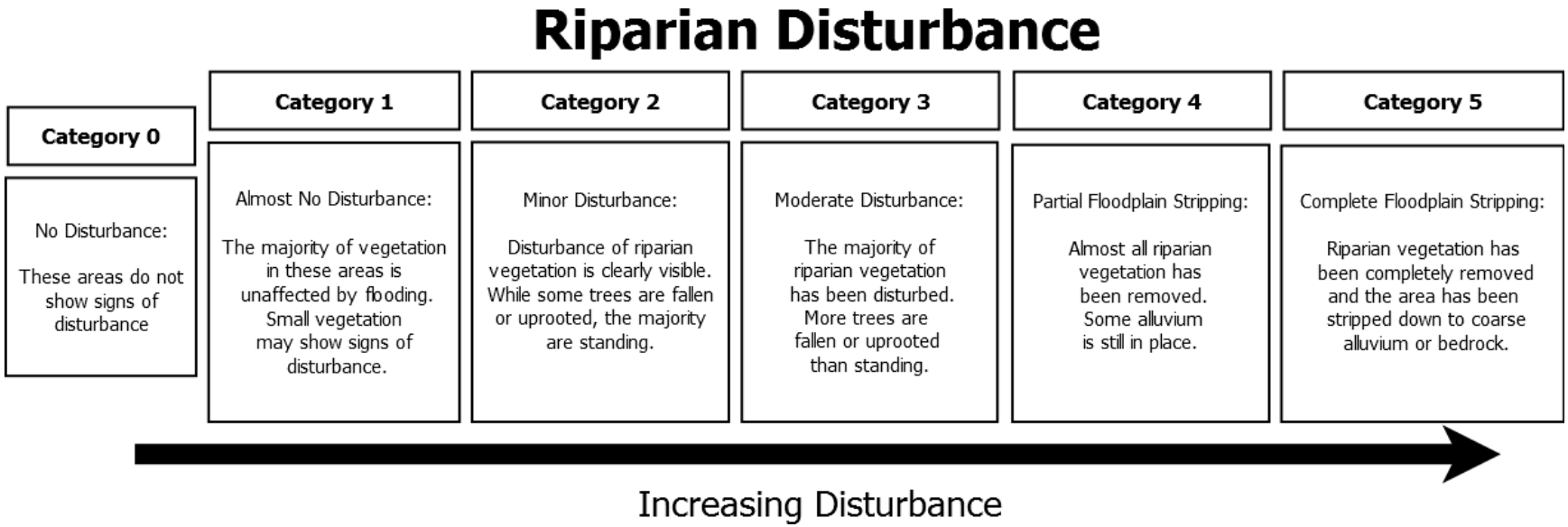

Figure 4 Riparian Disturbance Categories. A proposed scheme of categorizing disturbance. The categories range from least disturbance (1) to most disturbance (6).

Category 0 represents areas of no change and was mapped and calculated by subtracting the riparian disturbance layer from the FEMA floodway layer.

Category 1 represents areas of almost no disturbance, areas which show signs of disturbance such as minor scour and minimal vegetation disturbance. Tree stands remain robust and areas with small vegetation as well as grassy areas remain vegetated.

Category 2 represents areas which show signs of minor disturbance. In these areas, some trees have fallen and/or been uprooted, but the majority of vegetation remains in place. Tree stands and large herbaceous vegetation remain in place but has been thinned.

Category 3 represents areas which show signs of moderate disturbance. A significant amount of vegetation is present in these areas. However, the majority of vegetation has been disturbed. Some uprooted trees have been knocked down but still remain in place and very few trees may remain standing. Herbaceous vegetation has been thinned, knocked down, or completely removed from these areas.

Category 4 represents areas which were previously covered in vegetation and have been partially stripped. In these areas, substantial disturbance can be seen. The majority of vegetation has been removed. However, the area has not necessarily been stripped to its most resistant layer and some vegetation such as large trees remain but have been uprooted.

Finally, Category 5 represents areas which exhibit complete floodplain stripping. Category 5 areas are severely disturbed areas which were previously covered in vegetation and have been stripped down to coarse alluvium or bedrock.

The following describes the categories for the geomorphic disturbance. The categories cover both erosion and deposition which occurred during the event. The

classification is denoted by categories A, B, C, and D. Category A represents areas within the FEMA floodway layer which do not show signs of geomorphic disturbance. Category B shows areas which have been slightly eroded including areas on the floodplain away from the channel which show minor isolated scour. Category B also represents fine sediments deposited across a wide area not creating new features or adding to any features. Category C represents moderate erosion or deposition. This includes existing features which have been deepened or widened by the flooding as well as moderate deposition of fine to course sediments on the floodplain or the expansion of already existing features in the channel like the inside bends of meanders. Category D shows major erosion or scour including new chutes, which have been excavated by the floods, and or areas of extensively widened channel. Category D also represents major deposition of course materials, debris, and alluvium creating new forms such as a point bar inside the channel. An example of both the primary and nested categories can be seen in Figure 6.

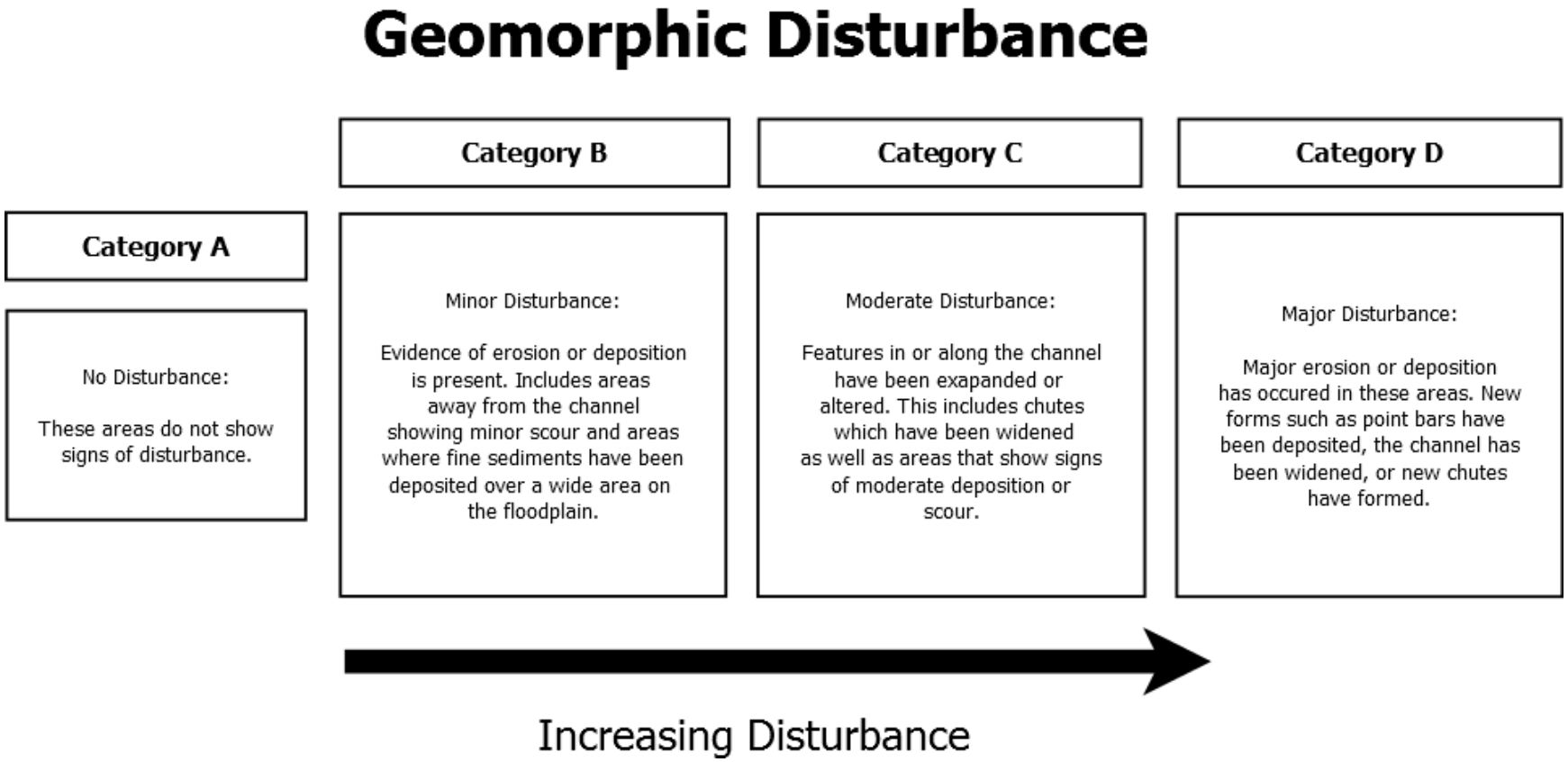

Figure 5 Geomorphic Disturbance Categories. Category A represents no disturbance and Categories B–D represent increasing erosional and depositional disturbance.

In addition to the riparian and geomorphic disturbance layers, I also digitized the pre- and post- flood channel along the entire study area. Along areas of the channel which were completely dry in the pre-flood imagery, I made the pre-flood channel extent match the post-flood layer extent to minimize any error which would have been caused by attempting to estimate the channel width.

For all digitized layers, the valley-width of the study area I digitized was mostly constrained by the 500 year FEMA floodplain layer. The exception to this was in a few areas where disturbance was visible outside of the 500-year layer. At tributary confluences, the 500-year layer extended well upstream into the tributary. For this reason, the 500-year layer was clipped near the confluences to match the approximate distance of the surrounding area. A no-change layer for both riparian and geomorphic disturbance was created by using the Erase tool in ArcMap to subtract the digitized layers from the floodway layer. The Erase tool was then used with combined floodplains and combined disturbance layers to identify the digitized areas which fell outside of the 500-year floodplain. Finally, a river centerline was manually digitized using the USGS Level II DEM as a reference. All digitization was performed at a 1:750 scale to ensure continuity throughout the process.

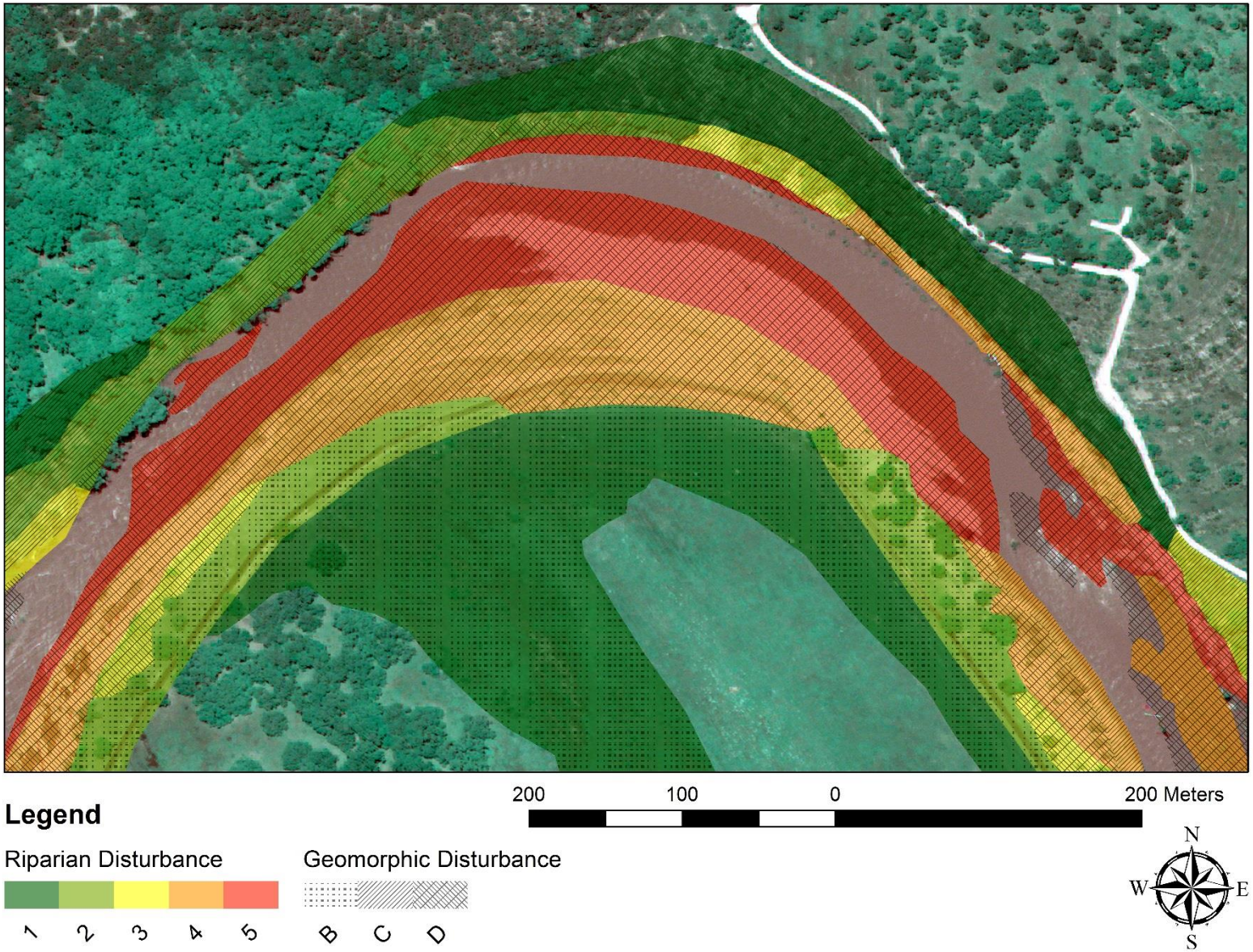

Figure 6 Disturbance Categorization Example. Pre- and post-flood imagery of a section of The Blanco River are shown (top) along with the primary and nested categories overlaid on the imagery (bottom right).

e. Disturbance Calculation

A goal of this study is to map, categorize, and quantify disturbance patterns along the river. After mapping and categorization were complete, I quantified the total areas of each category of disturbance within the FEMA floodplain layers.

The area calculations were broken down by category for both riparian and geomorphic disturbance. I queried the individual categories, separated them into feature classes and calculated their areas. Next, the percentages of each disturbance layer per floodplain layer were calculated by clipping each category layer to the floodplain layer in which it lies and dividing the intersecting disturbance area by the total disturbance area for each Category. This process was then repeated for geomorphic disturbance to find the proportion of each geomorphic category per floodplain layer relative to total geomorphic disturbance. Finally, intersections were performed between the riparian and geomorphic layers to calculate the area of each riparian category per geomorphic category.

To calculate areas of channel widening, I subtracted the digitized pre-flood channel layer from the digitized post-flood channel layer. However, this did not account for areas of the river which became narrower post-flood due to deposition. To account for these areas, I subtracted the post-flood area from the pre-flood area. I combined the two layers into a single layer of post-flood channel net loss and net gain.

f. Analysis Methods

To further examine the relationship between the river's physiography and disturbance, variables including channel width, floodway width, slope, stream power, floodway specific stream power, and channel specific stream power were measured. Circular buffers were created along the river and used to clip the disturbance layers and

create a snapshot of the total disturbance area as well as the relative proportion of disturbance per sample that occurred in each given area along the river. These areas were then compared against the measured variables to check for trends.

First, points were created systematically along the river centerline at a 10-meter interval beginning upstream and ending at the downstream study area extent. Because ArcGIS does not have a native tool for creating points along a line at regular intervals, I used the Create Points on Line tool, an unofficial tool on arcgis.com created by Ian Broad (2014). The Extract to Values Points tool was then used to derive elevation values from the USGS level II DEM and assign them to corresponding points.

Next, evenly-spaced transect lines running perpendicular to the river centerline at an interval of 10 meters were created. To create the transect lines, I used the Linear Sampling Toolbox, an unofficial ArcGIS tool created by Vini Indriasari (2015) from the University of Texas at Dallas. The toolbox includes a script tool called Transect sampling which creates transect lines along a polyline at a user-specified interval and length. After creation, the transect lines were clipped to match the post-flood channel extent. By clipping the transect lines and calculating their shape length, I effectively created a feature class which measures channel width along the river every ten meters.

After the elevations and channel width has been calculated along the river, I used the points at the intersection of the measured transect lines and the river centerline as centroids for buffers which were created for taking samples of disturbance along the river. Before the sample circles were created however, I used the Create Routes tool and the Locate Features along Routes tool in the Linear Referencing toolbox in ArcMap to calibrate the river centerline and associate measures with each sampling point. The

measure begins at 0 meters upstream and ends at approximately 55,800 meters downstream. An attribute table containing each sample point's elevation and distance measurement was exported into Excel to create a graph representing the river's longitudinal profile. Extraneous points along the profile were removed to create a smooth profile as shown in Figure 7. Although Figure 7 uses points spaced every 10 meters to represent the longitudinal profile, elevation values were compared every 100 meters to calculate slope later in the process. I chose to use the larger distance interval for slope calculation due to the high variability between elevations with the 10 meter points which led to slope values as high as 45 percent between some points.

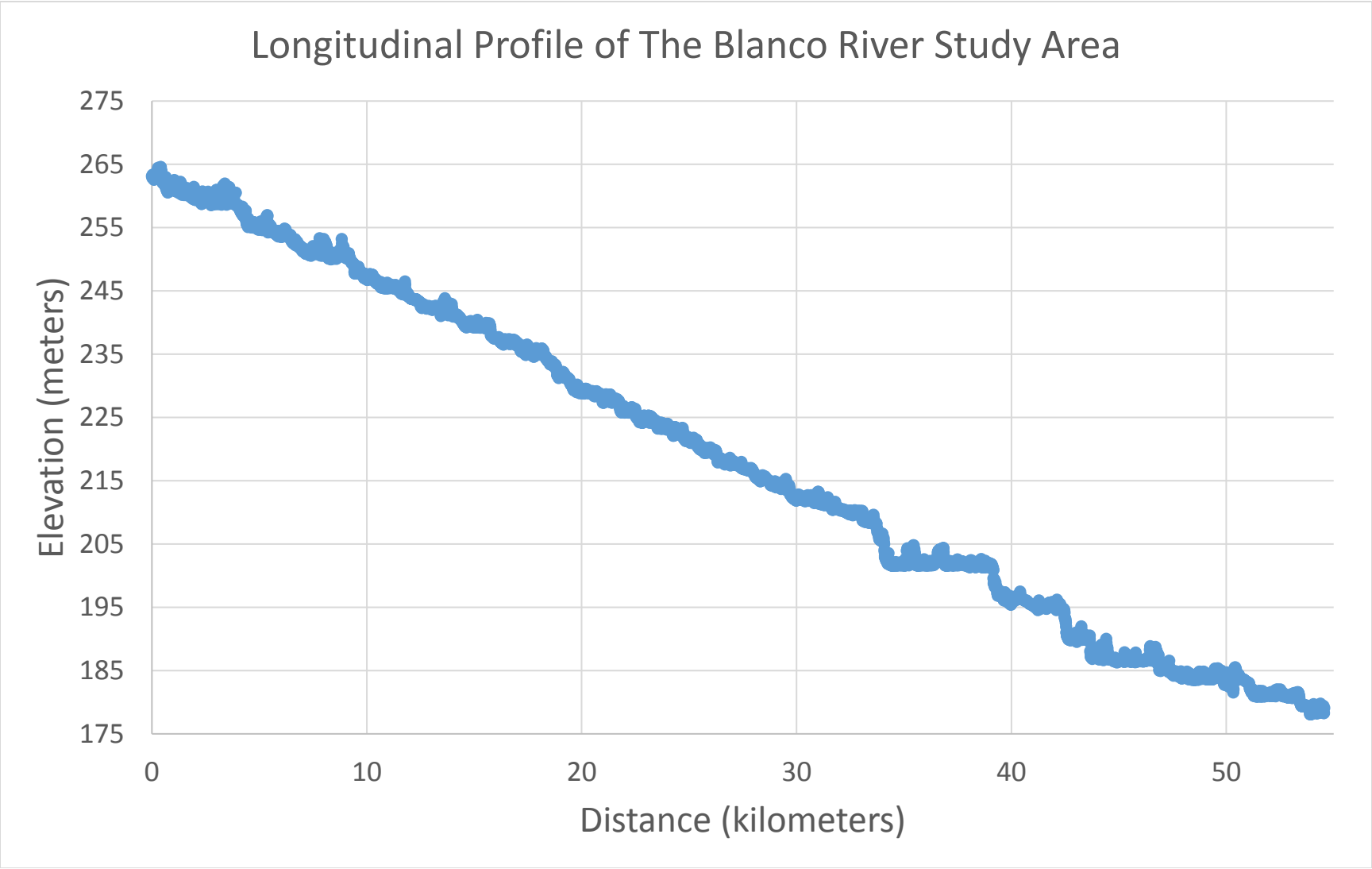

Figure 7 Longitudinal Profile of The Blanco River Study Area

Next I created the sample circles. I experimented with different shapes, sizes, and distance intervals to use for sampling. Although sample circles with larger buffers successfully accounted for most disturbances within the floodway and some outside of the floodway, they also extended outside of all floodplains in some areas picking up 'empty' areas of no data. This primarily occurred in areas where the river bended sharply or the natural geometry of the river results in the disturbance and/or the floodplain being unevenly distributed on the left or right side of the river. I also tried using elliptical and rectangular polygons to solve for the river geometry problem, but ultimately decided on circular polygons at an interval of 10 meters and a radius of 80 meters for sampling.

After the sample circles were constructed, both the riparian and geomorphic disturbance layers were clipped to each sample circle and the areas were recalculated per disturbance category. To account for the irregularities in the river and the no data issue, an extra Clip was added to the sampling process. After the disturbance was clipped to the sample circle, the sample circle was then clipped to match the extent of the disturbance. This eliminated all areas with no data in the sample. I then calculated the proportion of each category of disturbance relative to the total disturbance per sample.

To accomplish this calculation for the 5200 sample circles of the entire river, a custom Python script was written which creates a moving window that clips the disturbance layer to each sample circle, recalculates the areas of each category of disturbance within the circle, and appends the result to a master list. This script can be found in Appendix B. To analyze the relationship between channel width, valley width and each of the individual disturbance categories (riparian and geomorphic) a correlation

was performed on each of the relative disturbance categories against each other and against the channel and valley widths at each sample point along the river. A map of the sample circles can be seen in Figure 8.

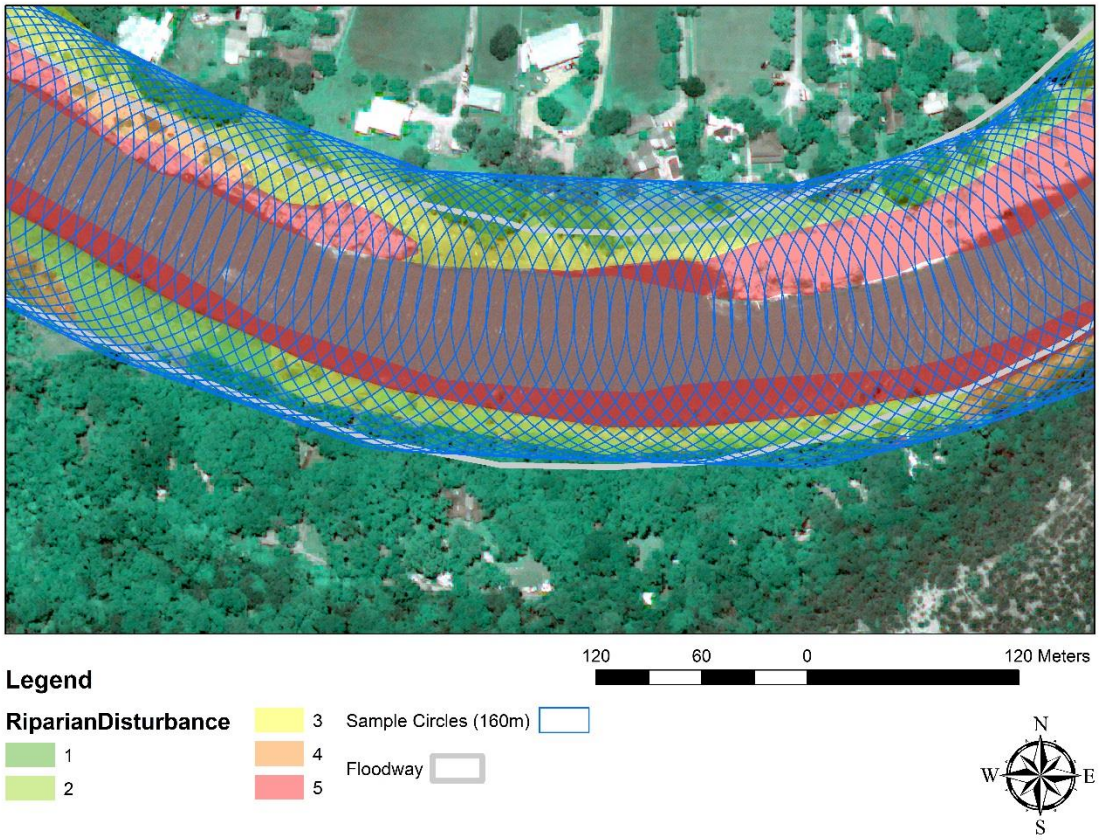

Figure 8 Sample Circle Illustration. An illustration of the 'sample circles' used to collect area per category measurements along the study area.

g. Hydrologic and Hydraulic Analysis

Stream power is a function of a river's discharge multiplied by the water's density, gravity, and slope. A river's stream power can be expressed as $\Omega = pgQS$ where Ω is stream power, p is the density of water (1000 kg/m3), g is acceleration due to gravity (9.8 m/s2), Q is discharge (m3/s), and S is the channel slope (Bagnold 1966). The only functioning stream gage was destroyed during the flood, however estimates of the event

are in the range of 4,955-5,097 m^3s^{-1} (USGS 08171300, NWIS 2016). I used the low end of the USGS estimated discharge (4,955 m^3s^{-1}) as an input to the stream power function which was applied at cross sections along the river every ten meters.

Because I was comparing various segments of the river, I needed to calculate the specific unit stream power for different segments of the river. Specific unit stream power can be calculated by dividing the river's stream power at a given area by the river's width in that area. Using the same 10 meter transect lines that I used with the channel width calculations, I clipped the transect lines using the FEMA floodway layer. The calculated lengths of the clipped transect lines represent the valley width and were used to standardize the specific stream power equation along the river. To improve accuracy of the slope values, I used the measure and elevation values I derived earlier to calculate the slope by drop in elevation over 100 meters per measure change along the river centerline. I chose to calculate the slope over 100 meter spans because the slope between 10 meter intervals was highly variable. I also removed the first 10 sample circles from the beginning and end of the study area because the circle extents were reaching outside of the study area.

The slope, channel width, and valley width values allowed me to calculate specific stream power along the entire study area every 10 meters. The results from the sampling circle method detailed in the previous section were correlated against stream power for each segment to compare specific stream power with disturbance.

IV. RESULTS

a. River Statistics

Table 1 shows the interpretations for correlation coefficients and their respective strengths which I will use throughout this paper. Values range from +/- 0.00 -0.19 in the 'Very Weak' category to +/- 0.80 – 1.0 in the 'Very Strong' category.

Table 2 is a summary of statistics describing the river within the extent of the study area. Channel elevation values range from a maximum of 80.6 meters to a minimum of 54.3 meters and averages 67.1 meters. Channel slope as a function of loss in elevation divided by distance between centerline points ranges from 0.0206 to less than 0.0001 averaging 0.0017. The channel width ranges from 180.6 meters to 5.6 meters at an average of 52.5 meters. The floodway width ranges from 601 meters to 66.7 meters at an average of 171.2 meters. Stream power ranges from 1,001,608 watts to 915 watts averaging 82,807 watts. Specific stream power normalized by channel width has a maximum value of 34,569 watts per meter, a minimum value of 22 watts per meter, and an average of 1,897 watts per meter. Specific stream power normalized by floodway width has a maximum of 5,809 watts per meter and a minimum of 9 watts per meter averaging 569 watts per meter. Calculated net gain and net loss (i.e. the difference in area between the pre-and post-flood channel area) were 793,048 m^2 and 58,652 m^2 respectively.

Correlation Coefficient	Interpretation
.00 - .19	Very Weak
.20 - .39	Weak
.40 - .59	Moderate
.60 - .79	Strong
.80 - 1.0	Very Strong

Table 1 Correlation Coefficients and Their Interpretations. (Owen 2015)

Table 3 shows a Pearson correlation of all river statistics in relation to each other. Statistically

significant values are denoted by ** in the table. The strongest significant relationship with elevation is floodway width which has a moderate negative correlation (r = -0.594). Channel width has a weak correlation with elevation (r = 0.365) and floodway specific stream power also has a weak correlation with elevation (r = 0.250). Slope, stream power, and channel specific stream power all have very weak, but significant relationships with elevation.

Floodway width does not correlate moderately or strongly with any river statistics having its strongest relationship with floodway specific stream power as it was used in the calculation. Channel width also does not correlate with any measurements or calculations aside from a negative correlation with channel specific stream power.

River Statistics			
	Min	Max	Average
Channel Width (m)	5.6	180.6	52.5
Floodway Width (m)	66.7	601.0	171.2
Stream Power (W)	915	1,001,608	82,807
Specific Stream Power (Channel) (W/m)	22	34,569	1,897
Specific Stream Power (Floodway) (W/m)	9	5,809	569
Elevation (m)	54.3	80.6	67.1
Slope	< 0.0001	0.0206	0.0017
Channel Net Loss and Gain			
Channel Net Loss (m^2)	793,048		
Channel Net Gain (m^2)	32,446		

Table 2 Descriptive Statistics for the River in the Study Area Extent and Calculated Channel Net Gain and Net Loss.

Finally, Slope has a complete linear relationship with stream power as it was the only variable input into the stream power functions and consequently correlates strongly with both channel and floodway specific stream power as it was the main input in those functions along with channel and floodway width. All values are statistically significant at the p = 0.01 level.

Pearson Correlation of River Measurements and Calculations

		Elevation	Floodway Width	Channel Width	Slope	Stream Power	Channel Specific Stream Power	Floodway Specific Stream Power
Elevation	Pearson Correlation	1	**-0.594****	**0.365****	0.069**	0.069**	-0.117**	0.250**
	Sig. (2-tailed)		0.000	0.000	0.000	0.000	0.000	0.000
Floodway Width	Pearson Correlation	**-0.594****	1	-0.125**	0.048**	0.048**	0.119**	-0.237**
	Sig. (2-tailed)	0.000		0.000	0.000	0.001	0.000	0.000
Channel Width	Pearson Correlation	**0.365****	-0.125**	1	0.041**	0.041**	**-0.299****	0.065**
	Sig. (2-tailed)	0.000	0.000		0.003	0.003	0.000	0.000
Slope	Pearson Correlation	0.069**	0.048**	0.041**	1	1.000**	**0.809****	**0.892****
	Sig. (2-tailed)	0.000	0.000	0.003		0.000	0.000	0.000
Stream Power	Pearson Correlation	0.069**	0.048**	0.041**	1.000**	1	**0.809****	**0.892****
	Sig. (2-tailed)	0.000	0.001	0.003	0.000		0.000	0.000
Channel Specific Stream Power	Pearson Correlation	-0.117**	0.119**	**-0.299****	**0.809****	0.809**	1	**0.649****
	Sig. (2-tailed)	0.000	0.000	0.000	0.000	0.000		0.000
Floodway Specific Stream Power	Pearson Correlation	**0.250****	**-0.237****	0.065**	**0.892****	**0.892****	**0.649****	1
	Sig. (2-tailed)	0.000	0.000	0.000	0.000	0.000	0.000	

*Table 3 Pearson Correlation of River Measurements and Calculations Taken Along the River in Relation to Each Other. **Is significant at the 0.01 level (2-tailed).*

b. Riparian Disturbance: Area Totals

Table 4 shows the total area of riparian disturbance calculated per category and separated by FEMA floodplain layer as well as the percentage of each category's disturbance area relative to the total area of each floodplain layer. The largest total disturbance area is Category 1 with an area of 2,390,415 m^2 and the smallest total disturbance area is Category 5 with an area of 1,112,288 m^2. Total disturbance area decreases with categories representing increasing severity. The no change category, Category 0, represents the largest area in all floodplains with an area of 18,204,985 m^2.

Category 0 (no change) also represents the largest total area within the floodway layer with an area 3,142,443 m^2 (35.7% of the Floodway) and Category 5 represents the smallest total area in the floodway with an area of 1,007,563 m^2 (11.4% of the Floodway).

Disturbance in the 100-year floodplain ranges from 957,341 m^2 (9.8% of the floodplain) in Category 1 to 92,354 m^2 (0.9% of the floodplain) in Category 5. The no change category, Category 0 represents an even larger portion of the 100-year floodplain with a total area of 7,321,478 m^2 (74.8% of the floodplain). Area of disturbance decreases as the severity of disturbance increases for the 100-year floodplain.

Disturbance in the 500-year floodplain ranges from 407,566 m^2 (4.8% of the floodplain) in Category 1 to 5,607 m^2 in Category 5 (0.1% of the floodplain). No change (Category 0) represents an area of 7,741,064 m^2 (91.7% of the floodplain). As with the 100-year floodplain, disturbance area decreases with increasing disturbance severity in the 500-year floodplain. Some disturbance in all 5 categories fell outside of all floodplain layers ranging from 241,448 m^2 (49.3% of the area outside of all floodplains) in Category

1 to 5,480 m^2 (1.1% of the area outside all floodplains) in Category 4. Disturbance area also decreases with disturbance severity outside of the FEMA floodplain layers apart from Category 5 which has approximately 1,300 m^2 more area outside of the floodplain than Category 4. Table 4 also shows decreasing areas of disturbance for all categories moving away from the channel. The exception to this trend is Category 1 which has an area of 957,341 m^2 (9.8% of the floodplain) in the 100-year floodplain compared to an area of 784,060 m^2 (8.9% of the floodway) in the floodway. Area of disturbance does however decrease in Category 1 with the 500-year floodplain and outside of the floodplain compared to the floodway and the 100-year floodplain layers. Additionally, Category 0, no change, increases moving away from the channel representing 3,142,443 m^2 (35.7% of the floodway) in the floodway and 7,741,064 m^2 (91.7% of the floodplain) in the 500-year floodplain.

Table 5 shows the percent disturbance relative to the total area of disturbance for each riparian category per floodplain. The same trends are seen in Table 5 as in Table 4, however Table 5 makes clear that categories of more severe disturbance, such as Category 4 and Category 5, show a larger decrease in area moving away from the channel than categories of less severe disturbance. The areas of Category 1 and Category 2 are relatively evenly distributed across the floodway layer and 100-year floodplain layer compared to the higher disturbance severity Categories which have most of their area represented in the floodway.

Riparian Disturbance Category Totals (Area in square meters, Percent of Floodplain)

Disturbance	Floodway		100 Year Floodplain		500 Year Floodplain		Outside Floodplain		Total Area
0	3,142,443	35.7%	7,321,478	74.8%	7,741,064	91.7%	0	0.0%	18,204,985
1	784,060	8.9%	957,341	9.8%	407,566	4.8%	241,448	49.3%	2,390,415
2	1,150,184	13.1%	811,950	8.3%	189,636	2.2%	173,542	35.5%	2,325,312
3	1,573,610	17.9%	422,364	4.3%	66,204	0.8%	62,244	12.7%	2,124,422
4	1,151,172	13.1%	180,175	1.8%	32,967	0.4%	5,480	1.1%	1,369,794
5	1,007,563	11.4%	92,354	0.9%	5,607	0.1%	6,764	1.4%	1,112,288

Table 4 Riparian Disturbance Category Totals. The total riparian disturbance per disturbance category in square meters and the percentage relative to the total area of each FEMA floodplain layer. Also included are the total disturbance which fell outside of all floodplain layers and the overall total disturbance per category.

Riparian Disturbance (Relative to Total Category Disturbance)

Disturbance	Floodway	100 Year	500 Year	Outside Floodplain
1	32.8%	40.0%	17.0%	10.1%
2	49.5%	34.9%	8.2%	7.5%
3	74.1%	19.9%	3.1%	2.9%
4	84.0%	13.2%	2.4%	0.4%
5	90.6%	8.3%	0.5%	0.6%

Table 5 Riparian Disturbance per Category Relative to Total Disturbance in that Category. The proportion of riparian disturbance per disturbance category separated by FEMA floodplain layer and expressed as a percentage as well as the proportion of disturbance which fell outside of all floodplain layers.

c. Geomorphic Disturbance: Area Totals

Table 6 shows the total area of riparian disturbance calculated per category separated by FEMA floodplain layer as well as the percent of disturbance area relative to the total area of each floodplain. Category A represents the largest total area with an area of 19,800,895 m^2 and Category D represents the least total area of disturbance with an area of 1,580,874 m^2. The total area of disturbance decreases across categories with increasing severity of disturbance except for Category B which has a larger total area than Category A.

For the floodway layer, total disturbance area ranges from 1,439,073 m^2 (16.3% of the floodway) in Category D to 2,122,030 m^2 (24.1% of the floodway) in Category C. Category C represents a larger total area in the floodway than Category B by approximately 60,000 m^2 and both Category B and Category C have a larger total area than Category D. The trend of increasing area per severity of disturbance seen in the riparian categories is not seen in the floodway column for geomorphic disturbance. The no change category, Category A, has the largest total area of 3,188,241 m^2 (36.2% of the floodway).

Total area of disturbance in the 100-year floodplain category ranges from 116,488 m^2 (1.2% of the floodplain) in Category D to 904,268 m^2 (9.2% of the floodplain) in Category B. Total disturbance area per category decreases for the 100-year floodplain with increasing disturbance severity and the no change category has the largest overall area of 8,433,580 m^2 (86.2% of the floodplain).

Total area of disturbance in the 500-year floodplain ranges from 13,567 m^2 (0.2% of the floodplain) in Category D to 187,573 m^2 (2.2% of the floodplain) in Category

B. Total disturbance area also decreases with increasing disturbance severity in the 500-year floodplain. No change again represents the largest area in the 500-year floodplain with an area of 8,179,074 (96.9% of the floodplain).

Total area of disturbance outside of the FEMA floodplain layers ranges from 11,746 m^2 (7.6% of the area outside of all floodplains) in Category D to 74,648 m^2 (48.5% of the area outside of all floodplains) in Category B. Category B and Category C both have more area outside of the floodplain than Category D.

Table 7 shows the percent disturbance relative to the total area of geomorphic disturbance for each category per floodplain. All categories have most of their disturbance represented within the floodway. Category B is more evenly distributed across the floodway and 100-year floodplain than the other two categories with 64.0% of its disturbance falling within the floodway and 28.1%. Category D is almost entirely represented within the floodway at 90.9%. All three categories decrease in percent area of disturbance moving away from the channel with their largest amounts of disturbance occurring in the floodway.

Geomorphic Disturbance Category Totals (Area in square meters, Percent of Floodplain)

Disturbance	Floodway		100 Year Floodplain		500 Year Floodplain		Outside Floodplain		Total Area
0	3,188,241	36.2%	8,433,580	86.2%	8,179,074	96.9%	0	0.0%	19,800,895
1	2,061,829	23.4%	904,268	9.2%	187,573	2.2%	67,507	43.9%	3,221,176
2	2,122,030	24.1%	331,264	3.4%	62,810	0.7%	74,648	48.5%	2,590,752
3	1,439,073	16.3%	116,488	1.2%	13,567	0.2%	11,746	7.6%	1,580,874

Table 6 Geomorphic Disturbance Category Totals. The total geomorphic disturbance per disturbance category in square meters separated by FEMA floodplain layers along with the total disturbance which fell outside of all floodplain layers and the overall total disturbance.

Geomorphic Disturbance (Percent Relative to Total Disturbance)

Disturbance	Floodway	100 Year	500 Year	Outside Floodplain
1	64.0%	28.1%	5.8%	2.1%
2	81.9%	12.8%	2.4%	2.9%
3	90.9%	7.4%	0.9%	0.7%

Table 7 Geomorphic Disturbance Relative to Total Disturbance. The proportion of geomorphic disturbance per disturbance category separated by FEMA floodplain layer and expressed as a percentage as well as the proportion of disturbance which fell outside of all floodplains.

d. Riparian and Geomorphic Disturbance Intersection

Table 8 summarizes the intersection between the geomorphic disturbance layer and the riparian disturbance layer. The intersection of the no change categories for both layers represents the largest area with 17,374,697 m^2 and the intersection between Category B and Category 5 represents smallest area of 14,498 m^2. The largest and smallest intersecting areas of Category A are 17,374,697 m^2 (Category 0) and 15,000 m^2 (Category 5). Intersecting areas of Category A decrease as the severity of the riparian categories increase.

Category B intersection areas range from 14,498 m^2 with Category 5 and 1,047,708 m^2 with riparian Category 2. Category 1 and Category 3 also have relatively large representations in Category B with 807,858 m^2 and 979,384 m^2 respectively. The no change and most severe disturbance riparian categories do not have large intersecting areas in this category.

Category C intersecting areas range from 103,042 m^2 in Category 1 to 881,471 m^2 in riparian Category 4. Category C mostly increases with increasing riparian disturbance except for Category 5 which decreases from Category 4.

Category D intersection areas range from 18,641 m^2 with Category 1 to 681,896 m^2 with Category 5. Aside from Category 0, the Category D intersecting area increases with increasing riparian disturbance severity. The total intersecting area of disturbance decreases with increasing geomorphic disturbance.

Table 9 shows the relative intersecting areas of the riparian and geomorphic disturbance layers for each category compared to the total intersecting area of the two layers. Apart from the no change layers, the highest relative intersecting area is that of

the two most severe disturbance categories, Category D from the geomorphic layer and Category 5 from the riparian layer with 43.3% of their total areas intersecting. Category B is relatively evenly distributed across Category 1, Category 2 and Category 3 and Category C is almost evenly distributed across Category 4 and Category 5.

Table 10 shows the results of a Pearson correlation calculated between the total area per sample circle of all riparian and geomorphic disturbance categories derived from the sampling process. Statistically significant correlation values at a p =0.01 level are denoted by * while values significant at p =0.05 are denoted by **. The geomorphic no change category, Category A, shows a moderate positive relationship with the riparian no change category, Category 0 (r =0.530, p =0.01). Category A also has a weak negative relationship with the most severe riparian disturbance category, Category 5 (r = -0.214, p =0.01). Category B has its strongest relationship with Category 3 (r =0.378, p =0.01), Category C has its strongest relationship with Category 4 (r =0.371, p =0.01), and Category D has its strongest relationship with Category 5 (r =0.388, p =0.01). Overall, the less severe geomorphic categories have weak negative relationships with the more severe riparian categories and the less severe riparian categories have no relationship or a negative relationship with the more severe geomorphic categories. This is seen with Category B which has a weak negative relationship with Category 5 (r = -0.302, p =0.01) and Category 1 and Category 2 which have no statistically significant relationship with Category D and weak negative relationships with Category C (r = -0.173 and r = -0.197, p =0.01).

Table 11 shows a non-parametric look at the relationships between riparian and geomorphic sample circle total areas using Spearman's Rho. Similar patterns are seen in Table 11 as in Table 10 such as the no change categories, Category A and Category 0 showing a moderate positive relationship ($r = 0.504$, $p = 0.01$) and the most severe disturbance categories, Category D and Category 5 having a weak positive relationship ($r = 0.377$, $p = 0.01$).

Disturbance Intersection Riparian and Geomorphic (Area in m2)

		Geomorphic Disturbance			
Riparian Disturbance		Category A	Category B	Category C	Category D
	0	**17,374,697**	168,263	207,111	455,156
	1	**1,284,534**	**807,858**	103,042	18,641
	2	**890,614**	**1,047,708**	196,892	48,554
	3	196,843	**979,384**	**798,229**	125,610
	4	39,210	201,049	**881,471**	246,347
	5	15,000	14,498	398,465	**681,896**
Total		19,800,898	3,218,759	2,585,211	1,576,204

Table 8 Disturbance Intersection: Riparian and Geomorphic. Total disturbance area of the riparian and geomorphic disturbance layers. Intersected in ArcGIS to show the total overlapping area per disturbance category. Expressed in square meters

Relative Intersection Area Riparian and Geomorphic (%)

		Geomorphic Disturbance			
Riparian Disturbance		Category A	Category B	Category C	Category D
	0	**87.7%**	5.2%	8.0%	28.9%
	1	6.5%	**25.1%**	4.0%	1.2%
	2	4.5%	**32.6%**	7.6%	3.1%
	3	1.0%	**30.4%**	**30.9%**	8.0%
	4	0.2%	6.2%	**34.1%**	15.6%
	5	0.1%	0.5%	15.4%	**43.3%**

Table 9 Relative Intersection Area: Riparian and Geomorphic. The proportion of intersecting area between disturbance categories and the total intersecting disturbance. Expressed as a percentage and divided by each geomorphic disturbance category as it relates to each riparian disturbance category.

Pearson Correlation of Total Area per Sample Circle between Disturbance Categories											
		CATA	CATB	CATC	CATD	CAT0	CAT1	CAT2	CAT3	CAT4	CAT5
CATA	Pearson Correlation	1.000	-0.277**	**-0.300****	-0.297**	**0.530****	-0.010	0.032*	-0.157**	-0.102**	-0.214**
	Sig. (2-tailed)		0.000	0.000	0.000	0.000	0.481	0.020	0.000	0.000	0.000
CATB	Pearson Correlation	-0.277**	1.000	**-0.411****	-0.237**	-0.166**	0.202**	0.280**	**0.378****	**-0.301****	**-0.302****
	Sig. (2-tailed)	0.000		0.000	0.000	0.000	0.000	0.000	0.000	0.000	0.000
CATC	Pearson Correlation	**-0.300****	-0.411**	1.000	**-0.363****	-0.207**	-0.173**	-0.197**	0.042**	**0.371****	0.108**
	Sig. (2-tailed)	0.000	0.000		0.000	0.000	0.000	0.000	0.002	0.000	0.000
CATD	Pearson Correlation	-0.297**	-0.237**	**-0.363****	1.000	-0.059**	-0.008	-0.009	-0.283**	0.068**	**0.388****
	Sig. (2-tailed)	0.000	0.000	0.000		0.000	0.557	0.497	0.000	0.000	0.000
CAT0	Pearson Correlation	**0.530****	-0.166**	-0.207**	-0.059**	1.000	-0.270**	-0.146**	-0.217**	-0.279**	-0.140**
	Sig. (2-tailed)	0.000	0.000	0.000	0.000		0.000	0.000	0.000	0.000	0.000
CAT1	Pearson Correlation	-0.010	0.202**	-0.173**	-0.008	-0.270**	1.000	-0.057**	-0.127**	-0.084**	-0.063**
	Sig. (2-tailed)	0.481	0.000	0.000	0.557	0.000		0.000	0.000	0.000	0.000
CAT2	Pearson Correlation	0.032*	0.280**	-0.197**	-0.009	-0.146**	-0.057**	1.000	-0.244**	-0.170**	-0.116**
	Sig. (2-tailed)	0.020	0.000	0.000	0.497	0.000	0.000		0.000	0.000	0.000
CAT3	Pearson Correlation	-0.157**	**0.378****	0.042**	-0.283**	-0.217**	-0.127**	-0.244**	1.000	-0.225**	**-0.486****
	Sig. (2-tailed)	0.000	0.000	0.002	0.000	0.000	0.000	0.000		0.000	0.000
CAT4	Pearson Correlation	-0.102**	**-0.301****	**0.371****	0.068**	-0.279**	-0.084**	-0.170**	-0.225**	1.000	-0.138**
	Sig. (2-tailed)	0.000	0.000	0.000	0.000	0.000	0.000	0.000	0.000		0.000
CAT5	Pearson Correlation	-0.214**	**-0.302****	0.108**	**0.388****	-0.140**	-0.063**	-0.116**	**-0.486****	-0.138**	1.000
	Sig. (2-tailed)	0.000	0.000	0.000	0.000	0.000	0.000	0.000	0.000	0.000	

*Table 10 Pearson correlation of Total Area per Sample Circle between Riparian and Geomorphic Disturbance Categories. Derived from the sampling process, this table shows the relationship in total area of all sample circles between disturbance categories. N = 5162 **Correlation is significant at the 0.01 level (2-tailed). *Correlation is significant at the 0.05 level (2-tailed)*

Spearman's Rho Correlation of Total Area per Sample Circle between Disturbance Categories											
		CATA	CATB	CATC	CATD	CAT0	CAT1	CAT2	CAT3	CAT4	CAT5
CATA	Correlation Coefficient	1.000	-0.253**	-0.266**	-0.277**	**0.504****	-0.023	0.073**	-0.158**	-0.033*	-0.147**
	Sig. (2-tailed)		0.000	0.000	0.000	0.000	0.093	0.000	0.000	0.019	0.000
CATB	Correlation Coefficient	-0.253**	1.000	-0.414**	-0.244**	-0.127**	0.160**	0.198**	**0.374****	-0.292**	-0.295**
	Sig. (2-tailed)	0.000		0.000	0.000	0.000	0.000	0.000	0.000	0.000	0.000
CATC	Correlation Coefficient	-0.266**	-0.414**	1.000	-0.346**	-0.160**	-0.188**	-0.178**	0.025	0.277**	0.090**
	Sig. (2-tailed)	0.000	0.000		0.000	0.000	0.000	0.000	0.074	0.000	0.000
CATD	Correlation Coefficient	-0.277**	-0.244**	**-0.346****	1.000	-0.068**	0.053**	0.020	-0.297**	0.092**	**0.377****
	Sig. (2-tailed)	0.000	0.000	0.000		0.000	0.000	0.144	0.000	0.000	0.000
CAT0	Correlation Coefficient	**0.504****	-0.127**	-0.160**	-0.068**	1.000	-0.241**	-0.111**	-0.200**	-0.240**	-0.054**
	Sig. (2-tailed)	0.000	0.000	0.000	0.000		0.000	0.000	0.000	0.000	0.000
CAT1	Correlation Coefficient	-0.023	0.160**	-0.188**	0.053**	-0.241**	1.000	-0.122**	-0.108**	-0.024	-0.022
	Sig. (2-tailed)	0.093	0.000	0.000	0.000	0.000		0.000	0.000	0.084	0.116
CAT2	Correlation Coefficient	0.073**	0.198**	-0.178**	0.020	-0.111**	-0.122**	1.000	-0.210**	-0.189**	-0.061**
	Sig. (2-tailed)	0.000	0.000	0.000	0.144	0.000	0.000		0.000	0.000	0.000
CAT3	Correlation Coefficient	-0.158**	0.374**	0.025	-0.297**	-0.200**	-0.108**	-0.210**	1.000	-0.203**	-0.506**
	Sig. (2-tailed)	0.000	0.000	0.074	0.000	0.000	0.000	0.000		0.000	0.000
CAT4	Correlation Coefficient	-0.033*	-0.292**	0.277**	0.092**	-0.240**	-0.024	-0.189**	-0.203**	1.000	-0.154**
	Sig. (2-tailed)	0.019	0.000	0.000	0.000	0.000	0.084	0.000	0.000		0.000
CAT5	Correlation Coefficient	-0.147**	-0.295**	0.090**	**0.377****	-0.054**	-0.022	-0.061**	**-0.506****	-0.154**	1.000
	Sig. (2-tailed)	0.000	0.000	0.000	0.000	0.000	0.116	0.000	0.000	0.000	

*Table 11 Spearman's Rho correlation of Total Area per Sample Circle between Riparian and Geomorphic Disturbance Categories. Derived from the sampling process, this table shows the relationship in total area of all sample circles between disturbance categories. N = 5162 **Correlation is significant at the 0.01 level (2-tailed). *Correlation is significant at the 0.05 level (2-tailed)*

e. River Statistics and Disturbance Correlation

Table 12 shows correlations between riparian disturbance area totals within each sample circle and river statistics\calculations. All riparian disturbance categories have a statistically significant relationship with floodway width at a 99% confidence level. Four categories have strong relationships with floodway width, Category 0 (r =0.774, p =0.01), Category 1 (r =0.769, p =0.01), Category 2 (r =0.851, p =0.01) and Category 3 (r =0.780, p =0.01). Category 4 and Category 5 show moderate positive relationships with floodway width at (r =0.467, p =0.01) and (r =0.560, p =0.01).

Channel width has very weak negative relationships with total sample circle disturbance area across all categories except for Category 0 and Category 5 which show very weak positive relationships. The strongest correlation between channel width and a disturbance category is a very weak negative with Category 3 (r = -0.196, p =0.01). Slope showed some very weak relationships with Category 0, Category 3, and Category 4. However, no statistically significant relationship was found for Category 1, Category 2, or Category 5. The Stream Power, Channel Specific Stream Power, and Floodway Specific Stream Power data also showed a mix of very weak relationships and insignificant relationships with the riparian disturbance categories.

Table 13 shows the non-parametric Spearman's Rho correlation for total area of riparian disturbance compared to river statistics and calculations. Table 13 follows the same overall pattern as Table 12 with the strongest relationships being in the Floodway Width column, the strongest being Category 0 (r =0.681, p =0.01). A weak negative relationship is present between Category 3 and Channel Width (r = -0.310, p =0.01). A

weak negative relationship is also seen between Floodway Specific Stream Power and Category 0 ($r = -0.305$, $p = 0.01$).

Tables 14 and 15 show the relationships between geomorphic disturbance categories and river measurements and calculations. Table 14 shows a Pearson Correlation while Table 15 shows Spearman's Rho. In Table 14, Elevation has a weak negative correlation with Category B and Category C ($r = -0.214$ and $r = -0.244$, $p = 0.01$). Category B also has a moderate positive correlation with floodway width ($r = 0.459$, $p = 0.01$) while the rest of the geomorphic categories have very weak negative relationships with floodway width. Category D has a weak relationship with channel width ($r = 0.317$, $p = 0.01$).

Table 15 also shows Category D having the strongest relationships with weak correlations between the category and Elevation/Channel Width at ($r = 0.353$ and $r = 0.337$, $p = 0.01$). Other very weak to weak relationships are seen in between most geomorphic categories, Slope, and Stream Power.

Pearson Correlation between River Statistics and Riparian Disturbance Categories								
		Elevation	Floodway Width	Channel Width	Slope	Stream Power	Channel Specific Stream Power	Floodway Specific Stream Power
CAT0	Pearson Correlation	**-0.417****	**0.774****	0.123**	0.049**	0.049**	0.004	-0.168**
	Sig. (2-tailed)	0.000	0.000	0.000	0.000	0.000	0.781	0.000
CAT1	Pearson Correlation	**-0.437****	**0.769****	-0.143**	-0.013	-0.013	0.038**	-0.187**
	Sig. (2-tailed)	0.000	0.000	0.000	0.362	0.362	0.006	0.000
CAT2	Pearson Correlation	**-0.487****	**0.851****	-0.080**	0.016	0.016	0.081**	-0.201**
	Sig. (2-tailed)	0.000	0.000	0.000	0.249	0.250	0.000	0.000
CAT3	Pearson Correlation	**-0.415****	**0.780****	-0.196**	0.048**	0.048**	0.122**	-0.151**
	Sig. (2-tailed)	0.000	0.000	0.000	0.001	0.001	0.000	0.000
CAT4	Pearson Correlation	-0.259**	0.467**	-0.074**	0.081**	0.081**	0.136**	-0.082**
	Sig. (2-tailed)	0.000	0.000	0.000	0.000	0.000	0.000	0.000
CAT5	Pearson Correlation	**-0.420****	**0.560****	0.054**	0.022	0.022	0.028*	-0.166**
	Sig. (2-tailed)	0.000	0.000	0.000	0.109	0.109	0.047	0.000

*Table 12 River Statistics, Stream Power, and Riparian Disturbance Pearson Correlation. This table shows the relationships between riparian disturbance categories and river measurements and calculations. N = 5161. **. Correlation is significant at the 0.01 level (2-tailed). *. Correlation is significant at the 0.05 level (2-tailed).*

Spearman's Rho Correlation between River Statistics and Riparian Disturbance Categories								
		Elevation	Floodway Width	Channel Width	Slope	Stream Power	Channel Specific Stream Power	Floodway Specific Stream Power
CAT0	Correlation Coefficient	**-0.483****	**0.681****	0.003	-0.089**	-0.089**	-0.068**	-0.305**
	Sig. (2-tailed)	0.000	0.000	0.838	0.000	0.000	0.000	0.000
CAT1	Correlation Coefficient	**-0.344****	**0.541****	-0.116**	-0.060**	-0.060**	0.002	-0.259**
	Sig. (2-tailed)	0.000	0.000	0.000	0.000	0.000	0.911	0.000
CAT2	Correlation Coefficient	**-0.400****	**0.602****	-0.146**	-0.027*	-0.028*	0.039**	-0.243**
	Sig. (2-tailed)	0.000	0.000	0.000	0.048	0.048	0.005	0.000
CAT3	Correlation Coefficient	**-0.410****	**0.562****	-0.310**	0.031*	0.031*	0.141**	-0.173**
	Sig. (2-tailed)	0.000	0.000	0.000	0.024	0.024	0.000	0.000
CAT4	Correlation Coefficient	-0.200**	**0.501****	-0.029*	0.036*	0.036*	0.063**	-0.122**
	Sig. (2-tailed)	0.000	0.000	0.036	0.011	0.010	0.000	0.000
CAT5	Correlation Coefficient	**-0.359****	**0.435****	0.026	-0.044**	-0.044**	-0.042**	-0.192**
	Sig. (2-tailed)	0.000	0.000	0.057	0.002	0.002	0.003	0.000

*Table 13 River Statistics, Stream Power, and Riparian Disturbance Spearman's Rho Correlation. This table shows the relationships between riparian disturbance categories and river measurements and calculations. N =5161. **. Correlation is significant at the 0.01 level (2-tailed). *. Correlation is significant at the 0.05 level (2-tailed).*

Pearson Correlation between River Statistics and Geomorphic Disturbance Categories								
		Elevation	Floodway Width	Channel Width	Slope	Stream Power	Channel Specific Stream Power	Floodway Specific Stream Power
CATA	Pearson Correlation	0.059**	-0.164**	0.198**	-0.131**	-0.131**	-0.186**	-0.061**
	Sig. (2-tailed)	0.000	0.000	0.000	0.000	0.000	0.000	0.000
CATB	Pearson Correlation	**-0.214****	**0.459****	**-0.261****	0.001	0.001	0.100**	-0.109**
	Sig. (2-tailed)	0.000	0.000	0.000	0.934	0.936	0.000	0.000
CATC	Pearson Correlation	**-0.244****	-0.090**	-0.176**	0.058**	0.058**	0.134**	0.036**
	Sig. (2-tailed)	0.000	0.000	0.000	0.000	0.000	0.000	0.010
CATD	Pearson Correlation	0.313**	-0.104**	**0.317****	0.032*	0.032*	-0.102**	0.065**
	Sig. (2-tailed)	0.000	0.000	0.000	0.022	0.022	0.000	0.000

*Table 14 River Statistics, Stream Power, and Geomorphic Disturbance Pearson Correlation. This table shows the relationships between geomorphic disturbance categories and river measurements and calculations. N = 5161. **. Correlation is significant at the 0.01 level (2-tailed). *. Correlation is significant at the 0.05 level (2-tailed).*

Spearman's Rho Correlation between River Statistics and Geomorphic Disturbance Categories								
		Elevation	Floodway Width	Channel Width	Slope	Stream Power	Channel Specific Stream Power	Floodway Specific Stream Power
CATA	Correlation Coefficient	0.055**	-0.165**	**0.246****	-0.117**	-0.117**	-0.189**	-0.057**
	Sig. (2-tailed)	0.000	0.000	0.000	0.000	0.000	0.000	0.000
CATB	Correlation Coefficient	-0.196**	**0.344****	**-0.235****	-0.006	-0.006	0.081**	-0.135**
	Sig. (2-tailed)	0.000	0.000	0.000	0.658	0.657	0.000	0.000
CATC	Correlation Coefficient	**-0.232****	0.007	**-0.233****	0.029*	0.028*	0.097**	0.039**
	Sig. (2-tailed)	0.000	0.593	0.000	0.040	0.041	0.000	0.005
CATD	Correlation Coefficient	**0.353****	-0.166**	**0.337****	0.061**	0.062**	-0.060**	0.105**
	Sig. (2-tailed)	0.000	0.000	0.000	0.000	0.000	0.000	0.000

*Table 15 River Statistics, Stream Power, and Geomorphic Disturbance Spearman's Rho Correlation. This table shows the relationships between geomorphic disturbance categories and river measurements and calculations. N = 5161 **. Correlation is significant at the 0.01 level (2-tailed). *. Correlation is significant at the 0.05 level (2-tailed).*

f. Relative Disturbance

In addition to total area per sample, the proportion of disturbance relative to the total disturbance per sample circle was also calculated. Table 16 shows the relationships of this relative disturbance calculation to river measurements and between disturbance categories. Overall, the relationships in this table are weaker than those in Table 12.

Elevation has a weak negative correlation with Category 1 and Category 2 ($r = -0.279$ and $r = -0.264$, $p = 0.01$) and a weak positive correlation with Category 4 ($r = 0.216$, $p = 0.01$). As with the total sample circle areas, the relative sample circle areas have a moderate positive relationship with the lower severity disturbance categories such as Category 1 ($r = 0.499$, $p = 0.01$) and Category 2 ($r = 0.466$, $p = 0.01$). The higher severity disturbance categories, Category 4 and Category 5, show a different relationship with floodway width than in Table 12. Whereas in Table 12, the two categories show a moderate positive relationship between total disturbance area and Floodway Width, Table 16 shows a weak negative relationship between floodway width and the area relative to the total area per sample circle (Category 4: $r = -0.184$, $p = 0.01$; Category 5 $r = -0.205$, $p = 0.01$). Category 0, no change, also has a negative relationship with Floodway Width ($r = -0.380$, $p = 0.01$). Channel Width shows an inverse pattern to the relationships seen in the Floodway Width column with Categories 1 – 3 having a negative relationship with Channel Width and Category 0, Category 4 and Category 5 having a positive relationship. Slope shows very weak to no relationship with the relative sample circle areas per riparian category. This is also the case with Channel Specific and Floodway Specific Stream Power with the strongest relationship being between the no change relative area and Channel Specific Stream Power at ($r = -0.204$, $p = 0.01$).

Table 17 shows the relative riparian disturbance area per category and their relationships to river statistics and calculations using Spearman's Rho. A moderate negative relationship ($r = -0.516$, $p = 0.01$) is seen between the riparian no change category and Floodway Width as well as a similar pattern in relationships between the Floodway Width and Channel Width columns with all categories having inverse relationships between the two. A mix between very weak relationships and no relationship is seen in the Slope, Stream Power, and Specific Stream Power columns.

Table 18 shows a Pearson correlation performed on the geomorphic relative disturbance categories and river statistics/calculations. Category B has a moderate positive relationship with Floodway Width ($r = 0.432$, $p = 0.01$) and a weak negative relationship with Channel Width ($r = -0.275$, $p = 0.01$). Category D shows an opposite trend having a weak negative relationship with Floodway Width ($r = -0.140$, $p = 0.01$) and a weak positive relationship with Channel Width ($r = 0.307$, $p = 0.01$). The geomorphic no change category, Category A, also correlates negatively with Floodway Width and positively with Channel Width ($r = -0.209$ and $r = 0.193$, $p = 0.01$). There are little to no relationships between relative area geomorphic categories and Slope/Stream Power with the strongest relationship being Category A and Stream Power ($r = -0.129$, $p = 0.01$). Table 19 shows Spearman's Rho calculations for relative geomorphic area and the stream statistics and calculations. Overall, the table follows the same patterns as Table 18 with weak overall relationships, the strongest being in the Floodway Width and Channel Width columns. However, there are some slightly stronger relationships such as Category D with Channel Width ($r = 0.334$, $p = 0.01$).

Pearson Correlation between River Statistics and Relative Riparian Disturbance Categories								
		Elevation	Floodway Width	Channel Width	Slope	Stream Power	Channel Specific Stream Power	Floodway Specific Stream Power
CAT0	Pearson Correlation	0.171**	**-0.380****	**0.282****	-0.084**	-0.084**	-0.204**	0.055**
	Sig. (2-tailed)	0.000	0.000	0.000	0.000	0.000	0.000	0.000
CAT1	Pearson Correlation	**-0.279****	**0.499****	-0.184**	-0.038**	-0.038**	0.042**	-0.156**
	Sig. (2-tailed)	0.000	0.000	0.000	0.006	0.006	0.003	0.000
CAT2	Pearson Correlation	**-0.264****	**0.466****	-0.153**	-0.002	-0.002	0.099**	-0.144**
	Sig. (2-tailed)	0.000	0.000	0.000	0.882	0.880	0.000	0.000
CAT3	Pearson Correlation	-0.045**	0.105**	**-0.264****	0.084**	0.084**	0.141**	0.045**
	Sig. (2-tailed)	0.001	0.000	0.000	0.000	0.000	0.000	0.001
CAT4	Pearson Correlation	0.216**	-0.184**	0.118**	0.071**	0.071**	0.023	0.085**
	Sig. (2-tailed)	0.000	0.000	0.000	0.000	0.000	0.097	0.000
CAT5	Pearson Correlation	0.044**	-0.205**	0.109**	-0.037**	-0.037**	-0.052**	0.021
	Sig. (2-tailed)	0.002	0.000	0.000	0.007	0.007	0.000	0.137

*Table 16 Relative Riparian Disturbance Pearson Correlations. This table shows the relationship between relative disturbance (as calculated per sample) and river measurements and calculations. The table also shows the relationship of relative disturbance between disturbance categories. N = 5161 **. Correlation is significant at the 0.01 level (2-tailed). *. Correlation is significant at the 0.05 level (2-tailed).*

Spearman's Rho Correlation between River Statistics and Relative Riparian Disturbance								
		Elevation	Floodway Width	Channel Width	Slope	Stream Power	Channel Specific Stream Power	Floodway Specific Stream Power
CAT0	Correlation Coefficient	0.132**	**-0.516****	0.280**	-0.050**	-0.050**	-0.157**	0.105**
	Sig. (2-tailed)	0.000	0.000	0.000	0.000	0.000	0.000	0.000
CAT1	Correlation Coefficient	**-0.257****	**0.467****	-0.122**	-0.057**	-0.057**	0.004	**-0.222****
	Sig. (2-tailed)	0.000	0.000	0.000	0.000	0.000	0.772	0.000
CAT2	Correlation Coefficient	**-0.278****	**0.472****	-0.126**	-0.023	-0.023	0.031*	-0.188**
	Sig. (2-tailed)	0.000	0.000	0.000	0.104	0.104	0.026	0.000
CAT3	Correlation Coefficient	-0.090**	0.098**	**-0.281****	0.052**	0.052**	0.139**	0.008
	Sig. (2-tailed)	0.000	0.000	0.000	0.000	0.000	0.000	0.579
CAT4	Correlation Coefficient	**0.209****	-0.079**	0.086**	0.058**	0.058**	0.030*	0.104**
	Sig. (2-tailed)	0.000	0.000	0.000	0.000	0.000	0.033	0.000
CAT5	Correlation Coefficient	0.010	-0.123**	0.118**	-0.042**	-0.042**	-0.081**	0.015
	Sig. (2-tailed)	0.453	0.000	0.000	0.003	0.003	0.000	0.267

*Table 17 Relative Riparian Disturbance Spearman's Rho Correlations. This table shows the relationship between relative disturbance (as calculated per sample) and river measurements and calculations. The table also shows the relationship of relative disturbance between disturbance categories. N = 5161 **. Correlation is significant at the 0.01 level (2-tailed). *. Correlation is significant at the 0.05 level (2-tailed).*

Pearson Correlation between River Statistics and Relative Geomorphic Disturbance Categories								
		Elevation	Floodway Width	Channel Width	Slope	Stream Power	Channel Specific Stream Power	Floodway Specific Stream Power
CATA	Pearson Correlation	0.095**	-0.209**	0.193**	-0.129**	-0.129**	-0.188**	-0.046**
	Sig. (2-tailed)	0.000	0.000	0.000	0.000	0.000	0.000	0.001
CATB	Pearson Correlation	-0.176**	**0.432****	-0.275**	0.009	0.009	0.106**	-0.095**
	Sig. (2-tailed)	0.000	0.000	0.000	0.523	0.524	0.000	0.000
CATC	Pearson Correlation	-0.223**	-0.113**	-0.171**	0.061**	0.061**	0.134**	0.050**
	Sig. (2-tailed)	0.000	0.000	0.000	0.000	0.000	0.000	0.000
CATD	Pearson Correlation	**0.349****	-0.140**	**0.307****	0.038**	0.038**	-0.093**	0.085**
	Sig. (2-tailed)	0.000	0.000	0.000	0.006	0.006	0.000	0.000

*Table 18 Relative Geomorphic Disturbance Pearson Correlations. This table shows the relationship between relative disturbance (as calculated per sample) and river measurements and calculations. The table also shows the relationship of relative disturbance between disturbance categories. N = 5161 **. Correlation is significant at the 0.01 level (2-tailed). *. Correlation is significant at the 0.05 level (2-tailed).*

Spearman's Rho Correlation between River Statistics and Relative Geomorphic Disturbance Categories								
		Elevation	Floodway Width	Channel Width	Slope	Stream Power	Channel Specific Stream Power	Floodway Specific Stream Power
CATA	Correlation Coefficient	0.092**	-0.203**	0.251**	-0.111**	-0.111**	-0.187**	-0.038**
	Sig. (2-tailed)	0.000	0.000	0.000	0.000	0.000	0.000	0.006
CATB	Correlation Coefficient	-0.176**	**0.335****	-0.253**	0.002	0.002	0.094**	-0.123**
	Sig. (2-tailed)	0.000	0.000	0.000	0.900	0.901	0.000	0.000
CATC	Correlation Coefficient	-0.209**	-0.019	-0.225**	0.028*	0.028*	0.093**	0.048**
	Sig. (2-tailed)	0.000	0.179	0.000	0.044	0.045	0.000	0.001
CATD	Correlation Coefficient	**0.387****	-0.190**	**0.334****	0.069**	0.070**	-0.052**	0.123**
	Sig. (2-tailed)	0.000	0.000	0.000	0.000	0.000	0.000	0.000

*Table 19 Relative Geomorphic Disturbance Spearman's Rho Correlations. This table shows the relationship between relative disturbance (as calculated per sample) and river measurements and calculations. The table also shows the relationship of relative disturbance between disturbance categories. N = 5161 **. Correlation is significant at the 0.01 level (2-tailed). *. Correlation is significant at the 0.05 level (2-tailed).*

V. DISCUSSION

a. River Measurements and Calculations

This study had two goals. The first goal was to identify biogeomorphic patterns of disturbance from catastrophic flooding and calculate their extents and the second was to examine how physiographic controls such as floodway width, channel width, and stream power contribute to disturbance. Sections a, b, c, and f discuss the area calculations and statistics presented in the results and how they relate to these two questions and sections d and e discuss patterns of disturbance which were identified during the digitizing process.

Of all the correlations between river measurements, the strongest was a moderate negative correlation between elevation and floodway width ($r = -0.594$, $p = 0.01$). This relationship can also be seen with the 100-year and 500-year floodplains which were much wider in the downstream portion of the study area than they were upstream.

Stream power varied widely along the study area ranging from 0 W to 1,001,608 W. Almost no correlation was found with stream power in relation to elevation, floodway width, or channel width. It is likely that the stream power calculation was inaccurate for two main reasons. The first reason is that the discharge input that was used for the stream power equation was the lower limit to the USGS estimate of peak flood discharge of 4,955 m^3s^{-1}. In reality, the discharge varied along the river and having a constant discharge input applied across the entire river. This means that the stream power calculation was more or less a function of slope. If absolute discharge measurements could be taken at multiple locations along the stream via stream gages, the stream power output would have been much more accurate. Unfortunately, the only functioning stream gage was broken during the flood making any absolute measurement of discharge

impossible. A new gage, USGS Blanco Rv at Crabapple Rd was placed at the intersection of Crabapple road and the Blanco River which could be useful in estimating discharge for future studies, especially in the upstream area. The second reason the calculation was inaccurate is due to the elevation values being derived from a DEM. Slope calculations derived via fieldwork would have been much more accurate and would have also resulted in better stream power estimates. Additionally, the slope which was measured from the DEM represents channel bed elevation and not water surface slope which is actually the input to the stream power equation.

I attempted to improve the stream power numbers and more accurately model slope by comparing elevation drop over 100 meters instead of 10 meters because there is too much variability in elevation between the 10 meter points. Despite reducing the slope and stream power calculations by a whole order of magnitude, there was still not an increased correlation between stream power and floodway width, channel width, or disturbance. Channel specific stream power does have a weak negative correlation ($r = -0.299$, $p = 0.01$) with channel width, increasing as channel width decreases, however it also had a strong correlation with slope ($r = 0.809$) strengthening the idea that, for this study, stream power is a function of slope.

I also expected channel width to show a stronger relationship with floodway width, however it only showed a weak negative correlation ($r = -0.125$, $p = 0.01$). As seen in Figure 9, the channel width did not vary in sync with the floodway in many places. The left map in Figure 9 shows the widest floodway in the study area. The right map shows a section of the river with a significantly smaller floodway having approximately the same channel width as the section in the left map. This is likely due to the Blanco having its

valley fixed in bedrock not allowing the fixed valley to migrate or widen while having its channel set in less resistant sediment allowing it to respond to biogeomorphic controls as mentioned by Patton and Baker (1977). Another factor that influenced artificially small channel widths were the dams along the river. The channel width directly downstream of the dams shrank considerably in most cases which is in line with Julian et al. (2016) and Graf (2006).

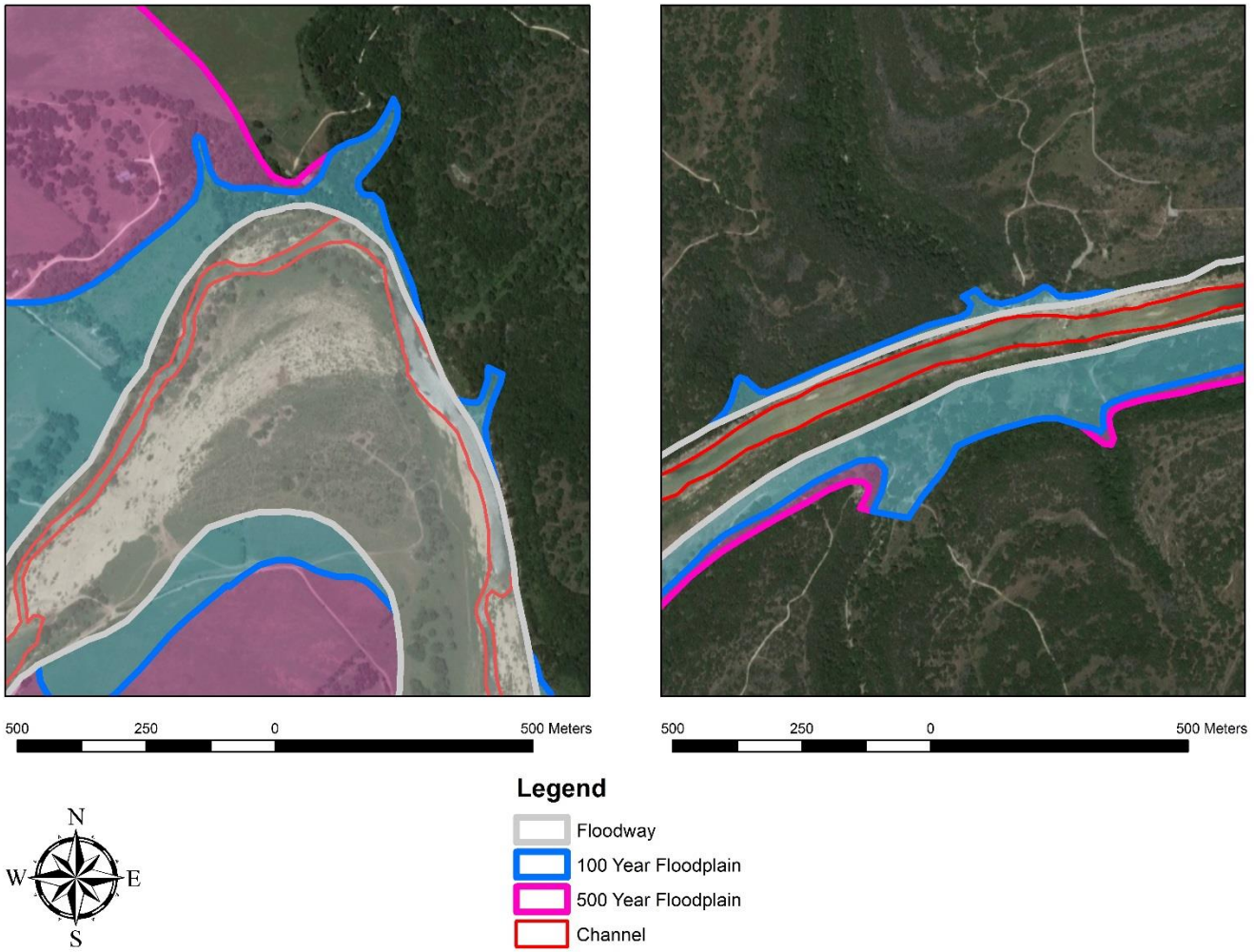

Figure 9 Channel width versus floodplain width. The left map shows the largest floodplain width in the study area. The right map shows an area with a smaller floodplain width. Both areas have similarly sized channels in that channel width does not have a strong relationship with floodplain width.

b. Disturbance Area Totals

Tables 4 and 5 show that most riparian disturbance was observed in the FEMA floodway layer. With Category 1 being the exception, disturbance area for all categories decreases moving away from the channel. This trend is especially evident with the most severe disturbance, Category 5. Category 5 has 90.6% of its disturbance occuring within the floodway with only 8.3% in the 100-year floodplain and 0.5% in the 500-year floodplain. This means that for severe disturbance, there is a sharp gradient of disturbance moving away from the channel. As the disturbance severity of each riparian category decreases however, the proportion of disturbance becomes more evenly distributed across and outside of the floodplains (Figure 10). This trend is also evident in the satellite and aerial imagery in that the most intense disturbance is often easy to locate in the channel, on islands in the channel, or directly along the channel with the less severe disturbance being mostly located on the floodplain outside of the channel.

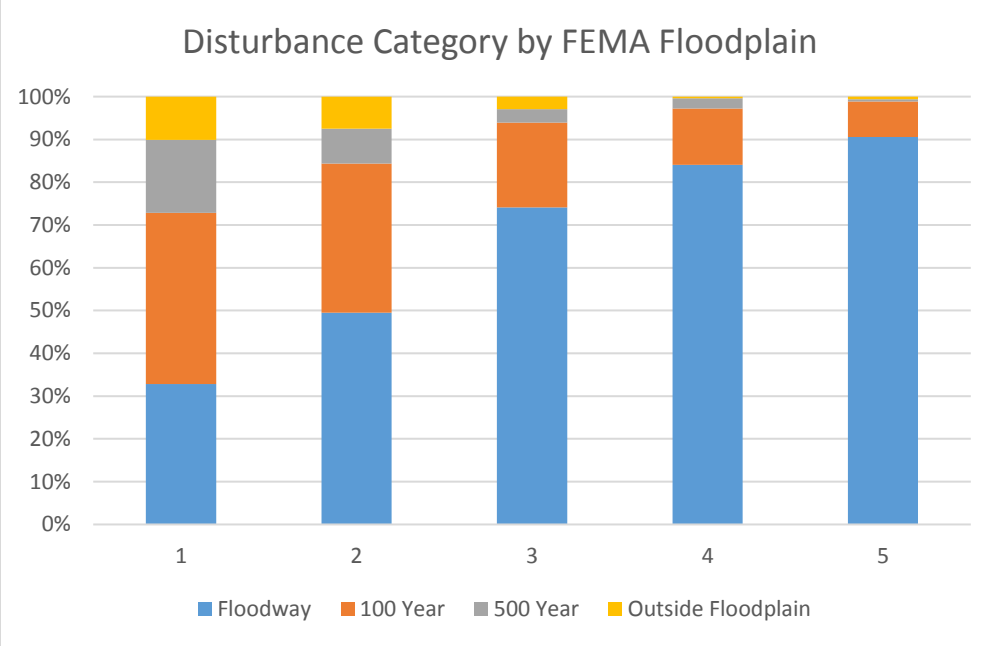

Figure 10 Disturbance Category by FEMA Floodplain. Disturbance shows a steep drop-off moving away from the channel.

Another trend seen with the riparian disturbance is that the total area of disturbance decreases as the severity of disturbance increases. This reinforces the idea that severe disturbance occurs directly in and along the channel while less severe disturbance occurs on the floodplain surface. The reason for this is that discharge is a main control for disturbance (Julian et al. 2016) and the majority of discharge occurs in the channel. The no change layer has more total area than all other categories for all floodplain layers. This means that, even within the floodway, most of the total area remains undisturbed. Geomorphic disturbance follows a similar total disturbance pattern to riparian disturbance with 91% of the most severe geomorphic disturbance, Category D, occurring near the channel in the floodway and showing a steep decline in area in the 100-year and 500-year floodplains with only 9.1% of its total disturbance occurring in those two floodplains or outside of the floodplain.

This pattern of the disturbance gradient moving outward from the channel is shown in Figures 11–13. Figure 11 shows the pre-flood channel, Figure 12 shows the post-flood channel, and Figure 13 shows the post-flood channel symbolized with geomorphic and riparian disturbance. The inside bend of the meander is completely stripped of vegetation and major geomorphic disturbance is evident. Moving inward, severe stripping is still evident, but some grass and vegetation is still present as seen in the orange Category 4 area. Further inward on the floodplain surface, the yellow area (Category 3) shows a tree stand that has been downed. The majority of trees have fallen or been uprooted but still remain in place. This is also the case across the river on the convex bank. Moving outward on both side of the river there are signs of minor geomorphic and riparian disturbance placing the areas in Category B and Category 1.

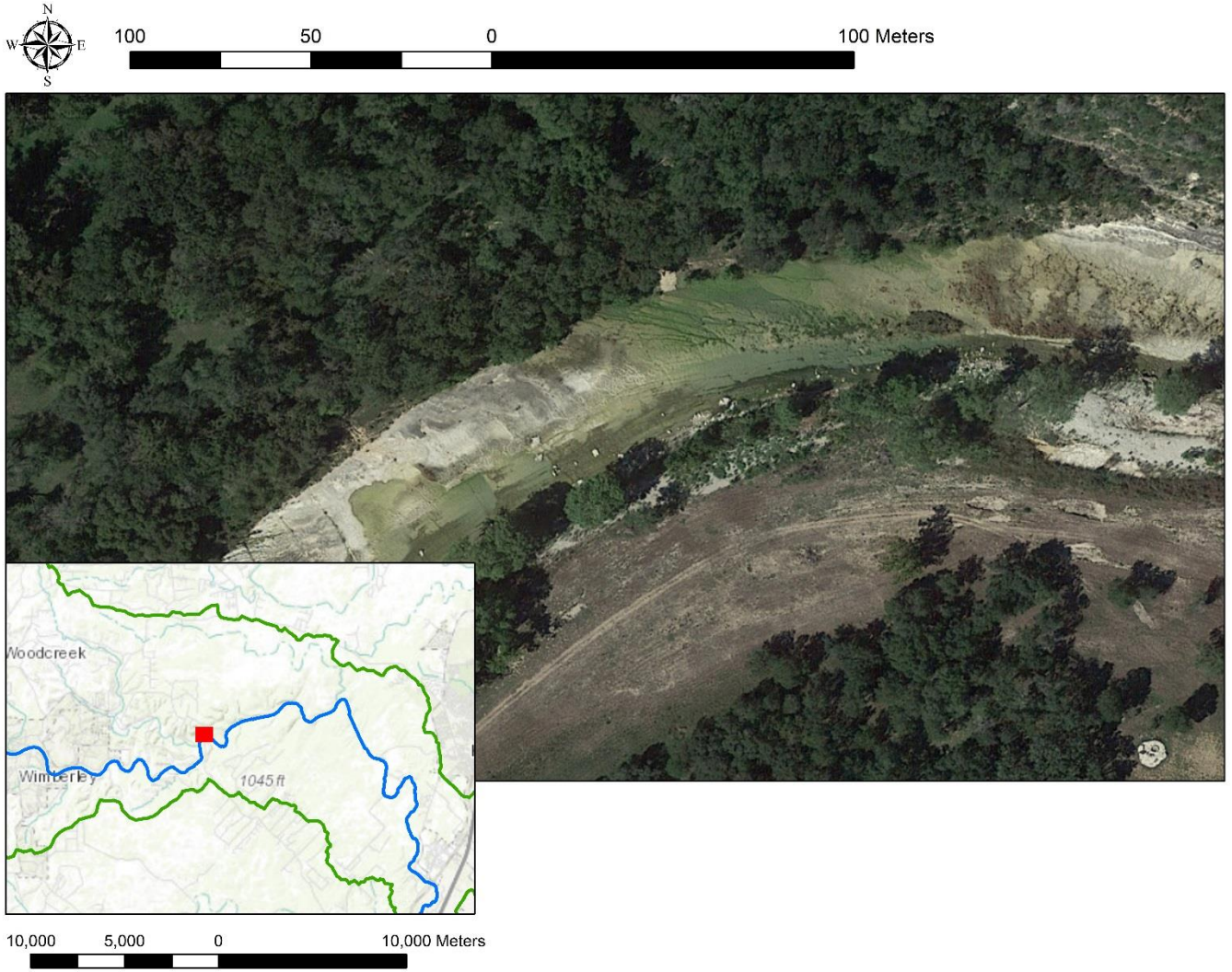

Figure 11 Pre-Flood Disturbance Gradient Example.

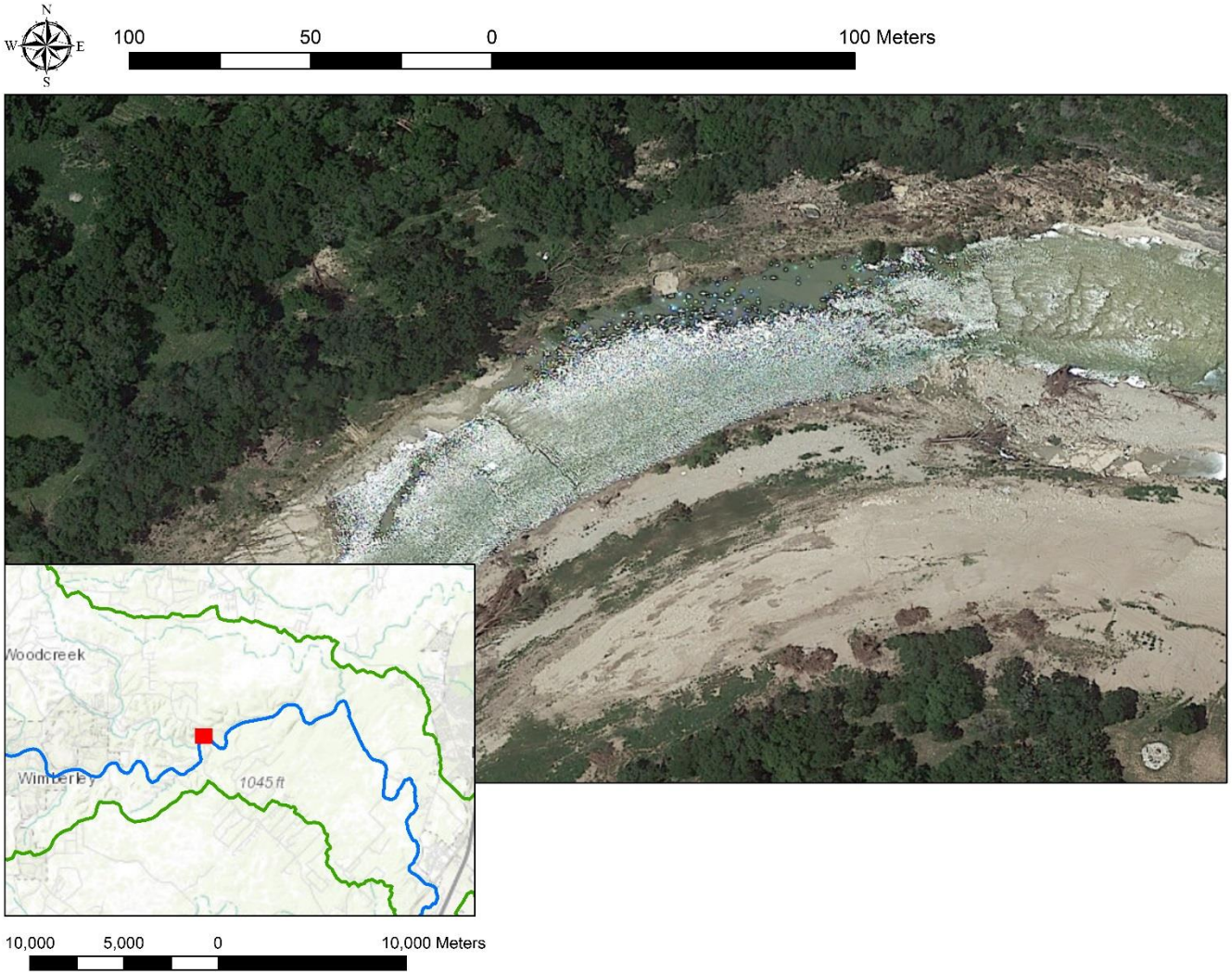

Figure 12 Post-Flood Disturbance Gradient Example.

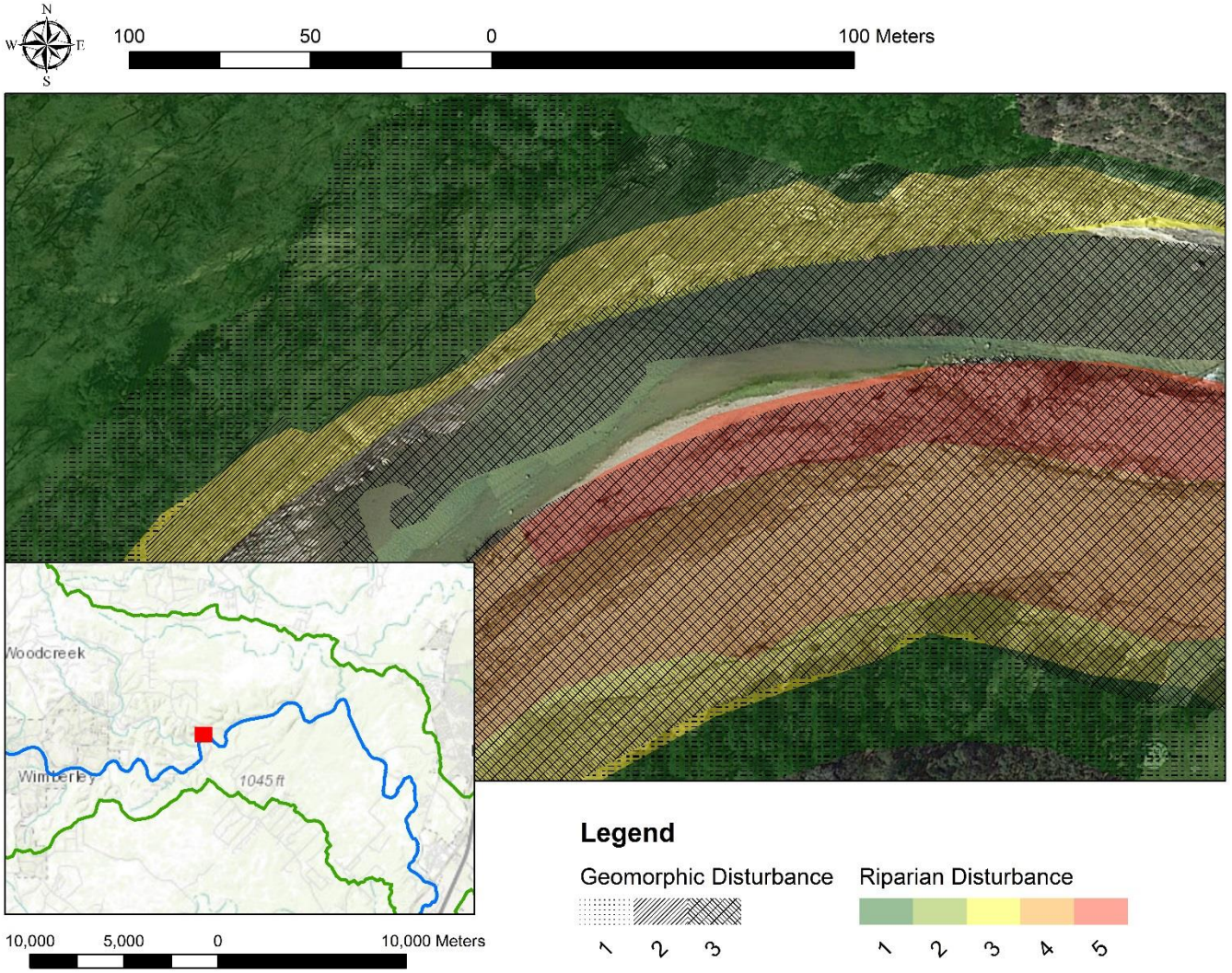

Figure 13 Post-Flood Disturbance Gradient Example Mapped and Categorized.

c. Riparian and Geomorphic Disturbance Intersections

Because the digitizing and categorization of disturbance involved subjectivity, it was important to verify my digitization. Tables 8 and 9 serve partially as this assessment. Because floodplain stripping is a biogeomorphic process which involves riparian and geomorphic change, a larger portion of the high severity geomorphic disturbance category should intersect spatially with the high severity riparian disturbance categories. Table 9 verifies that Category D intersects with Category 5 (43.3%) and Category 4 (15.6%) more than the less severe riparian categories. Category D is also well represented in Category 0 (28.9%) which seems counter intuitive, but this is due to Category 0 being a no change category and there being many areas in the floodway that experienced geomorphic change, but not riparian change. Category B should theoretically not intersect with Category 5 at all because areas that have been stripped should at least show moderate geomorphic disturbance, however 0.5% of the category intersects with Category 5 indicating a slight inaccuracy in digitization or categorization.

An interesting trend is seen between Categories B and C and Categories 1, 2 and 3. These areas represent areas that saw very little to moderate geomorphic and riparian disturbance. Areas that saw moderate geomorphic erosion or deposition but only minor to moderate riparian disturbance are on the cusp of the threshold of floodplain stripping or major disturbance. The flood event in these areas was strong enough to transport moderate amounts of sediment or cause moderate erosion but not strong enough to completely erode the river bank and remove vegetation. This is possibly due to root reinforcement and increased resistance from vegetation present in the area (Abernethy and Rutherford 2001; Anderson et al. 2006; Simon and Collison 2002).

Tables 10 and 11 also help to verify digitizing in that some of the strongest relationships seen in both the Pearson and Spearman's correlations are between the riparian and geomorphic no change categories and the most severe geomorphic and riparian disturbance categories. Significant relationships were also seen between the lower and middle severity geomorphic and riparian categories.

d. Floodplain Stripping, Meanders, and Other Disturbance Forms

Floodplain stripping was widespread throughout the entire study area occurring in or directly adjacent to the channel. Stripped areas were labeled Category 4, Category 5, and Category D. Because floodplain stripping is both a riparian and geomorphic process, the most severe geomorphic category (Category D) had a large amount of its area intersect with the two stripping categories (Categories 4 and 5). Table 9 shows that 58.9 percent of the area of Category D intersects with Categories 4 and 5.

An observed trend along the river was that many meanders, especially those with a sharp curve, experienced more severe disturbance and stripping on the inside of the meander bend while less severe disturbance occurring on the outside. These are possibly instances of convex bank erosion which occurs in areas with a resistant outer bank (Warner 1997). At the areas where this was observed, the outer bend of the meander has only a thin bank with limited vegetation and a steep limestone canyon wall. The meanders with the most severely disturbed convex banks occurred in the upstream study area where the river is more confined by canyons.

Meanders downstream tend to show less severe disturbance stripping was more sporadic downstream and confined to the channel. However, a greater total area was disturbed at the downstream reaches of the river. Along most sections of the river,

disturbance is of a higher intensity closer to the channel and less intense further away. This was not the case in areas where floodwaters cut across meanders. In these areas, high level chutes cutting across the inside of the meander experienced the highest severity of disturbance while the areas along the channel showed less severe signs of disturbance. Figure 14 shows an instance of across meander scour which was mentioned by Warner (1997). The stripping in Figure 14 is somewhat severe compared to other meanders along the river which showed signs of disturbance, but did not have vegetation stripped and removed from the floodplain. Isolated scour holes were also present on the floodplain and in the channel throughout the study area (Bourke 1994).

A feedback loop is possible here where vegetation is not able to establish itself on the high-level chutes which cut across meanders and the high-level floodways parallel to the channel which have been excavated by previous flood events. Both across meander scour and parallel chute erosion seem to follow this pattern of disturbance where flow follows the path of least resistance after entering a breached area along the channel bank. Because little or no vegetation is present in these areas, they are less resistant to subsequent flooding during high magnitude or catastrophic flood events. On the contrary, nearby areas which have robust vegetation cover are more resistant to floods (Anderson et al. 2006).

Floodplain construction is also evident in some areas where the bed load has been transported over the bank of the channel and deposited on the floodplain as mentioned by Bourke (1994). These blankets of sediment were categorized as both Category B and Category C according to the amount of sediment deposited. Another geomorphic form which was seen throughout the study area was the deposition of large gravel bars and

mid-channel islands. These bars and islands represent major geomorphic disturbance as new forms were created and were labeled Category D. The formation of these features lends credence to Patton and Baker (1977) who write about the major reworking of less resistant floodplain sediments within limestone channels with extremely resistant limestone bedrock. These mid-channel islands would be good candidates for monitoring in future studies to see if vegetation is able to establish itself on them before they are eroded by the next major flood event (Hupp 1992).

In many areas along the floodplain, small to large portions of the hardwood and herbaceous vegetation were either uprooted or completely removed yet the underlying grasses remained. These areas were labeled as riparian Category 2/Category 3 and geomorphic Category A/Category B. What is particularly interesting about these areas is that the disturbance threshold was large enough to remove small and large vegetation, but the erosional threshold was not large enough to remove the sediment and grasses as seen with the stripped areas. One possibility why this occurred was that the grasses increased the cohesiveness of the soils in these areas (Simon and Collison 2002), but the force exerted on larger vegetation was too much to keep their shallow roots in the ground. The grasses however are deeply rooted in comparison to their above ground parts which the flood waters act on.

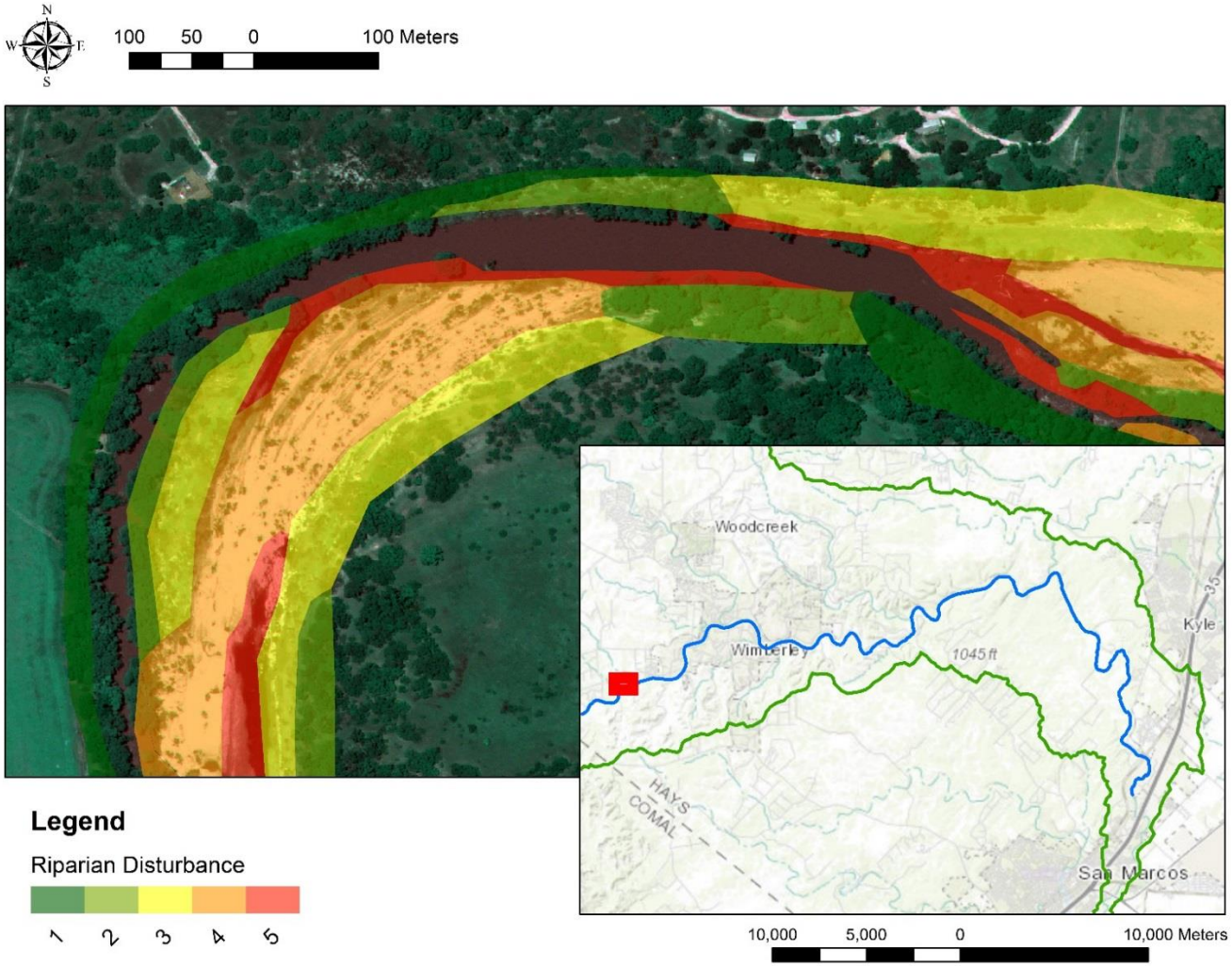

Figure 14 Across Meander Scour. An example of across meander scour as referenced in Warner (1997).

e. Tributary Confluences

Although there are a few major tributary confluences along the river, I could not identify any quantitative patterns of disturbance between them by comparing the sample circles at confluences to sample circles along other reaches of the study area. Visually however, I was able to find patterns of stripping as well as major riparian and geomorphic disturbance at most tributary confluences. Figures 15 and 16 show the confluence of Lone Man Creek and the Blanco River, Figure 17 shows the confluence of Cypress Creek and the Blanco River, and Figure 18 shows the confluence of Halifax Creek and the Blanco River. Similar patterns of floodplain stripping and major disturbance are seen at all three confluences despite them being located along various reaches of the upper, middle, and lower sections of the study area. The mechanisms which caused these patterns of disturbance are not entirely clear. It is possible that the disturbance was caused by discharge from the tributary, discharge from the main channel, or other factors such as the localized channel physiography/hydrology. There are too many variables and too small of a sample size to identify any trends with certainty. Some of the other varying factors at the confluences are the width of the tributary, the angle at which the tributary approaches the main channel, surrounding channel geometry, and land cover (Guillén-Ludeña et al. 2016).

Some interesting disturbance patterns were observed at the Lone Man Creek confluence where large amounts of sediment were deposited in the channel directly at the confluence and downstream. Two observations about this particular confluence which are worth investigation are the fact that the tributary is dammed directly upstream of the confluence and that the tributary meets the Blanco River at a right angle. Because the

Lone Man Creek tributary is dammed and dams typically limit sediment supplies downstream (Julian et al. 2016; Graf 2006), it can be hypothesized that the sediment deposited at the confluence and directly downstream came from the main channel. Additionally, the fact that the sediment was deposited directly at the confluence and downstream suggests that, at some point during the flood, the floodwaters were slowed here as the bedload was deposited. This confluence would be a good candidate for studies building on Julian et al. (2016) and Graf (2006) which would focus on the source of the sediment deposited at the confluence. It would also be a good location to examine Caskey et al. (2015) and Aguiar et al. (2016) by looking at the extent, heterogeneity and composition of riparian vegetation compared to upstream on both Lone Man Creek and the main channel.

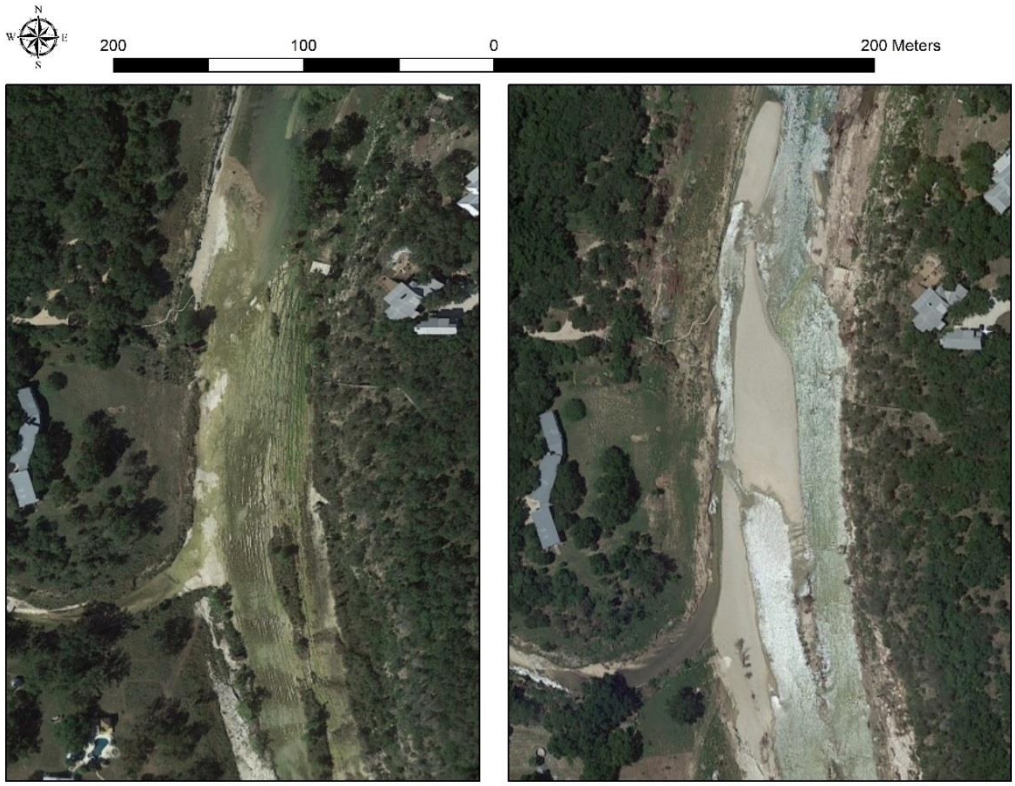

Figure 15 Deposition at Lone Man Creek. Large amounts of sediment deposited at the confluence of Lone Man Creek and the main channel.

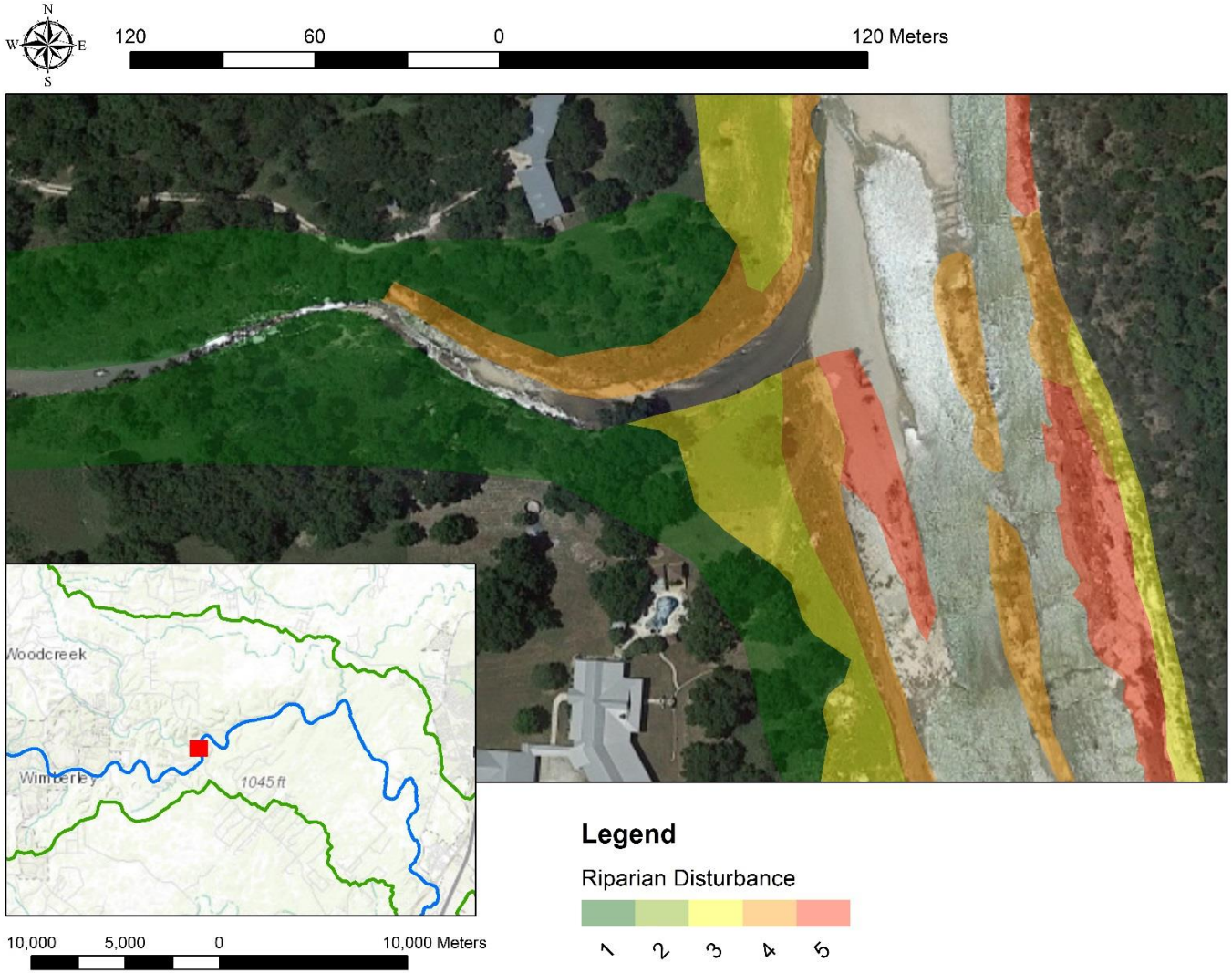

Figure 16 Lone Man Creek Confluence. Disturbance mapping at the confluence of Lone Man Creek and the Blanco River

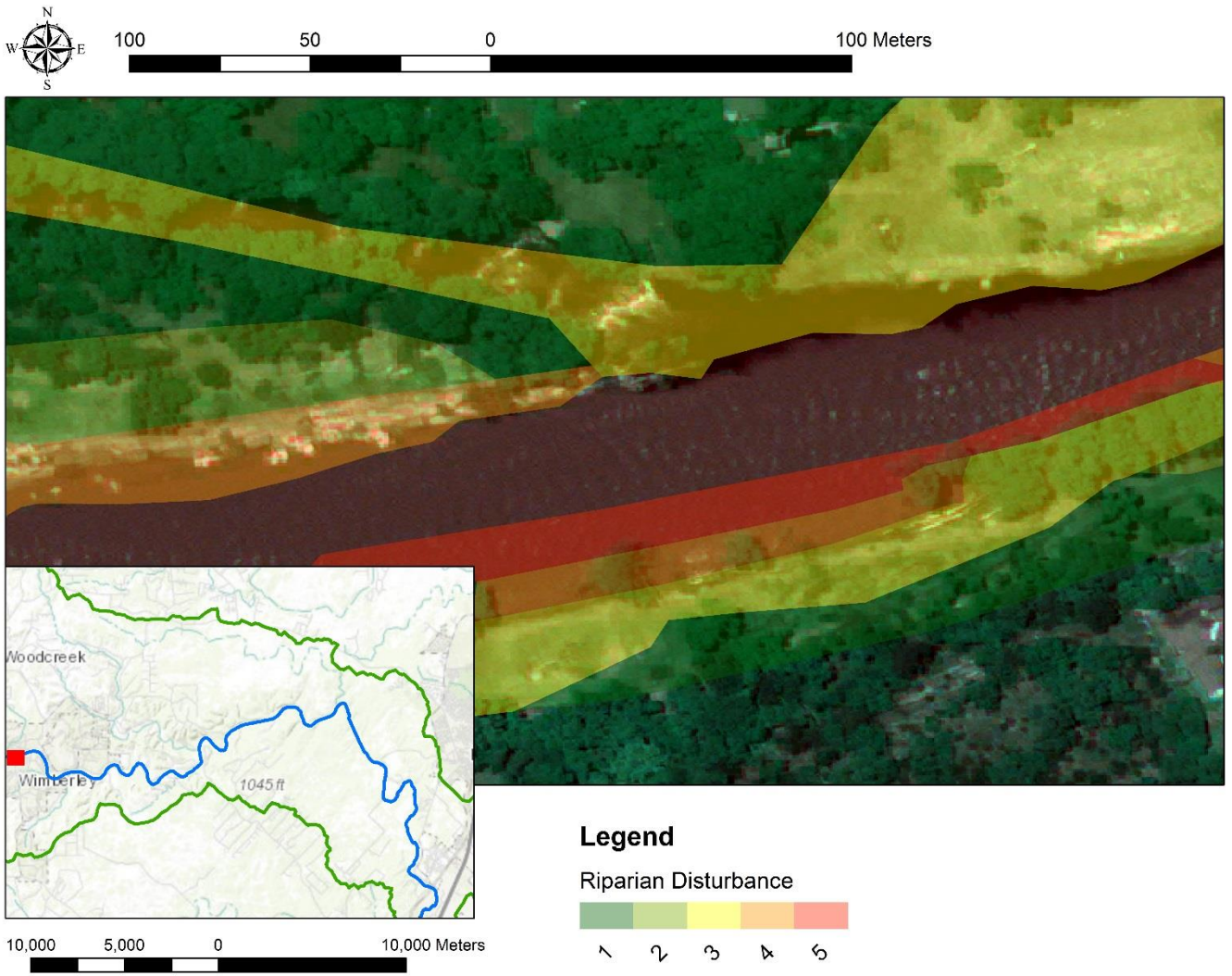

Figure 17 Cypress Creek Confluence. Disturbance mapping at the confluence of Cypress Creek and the Blanco River

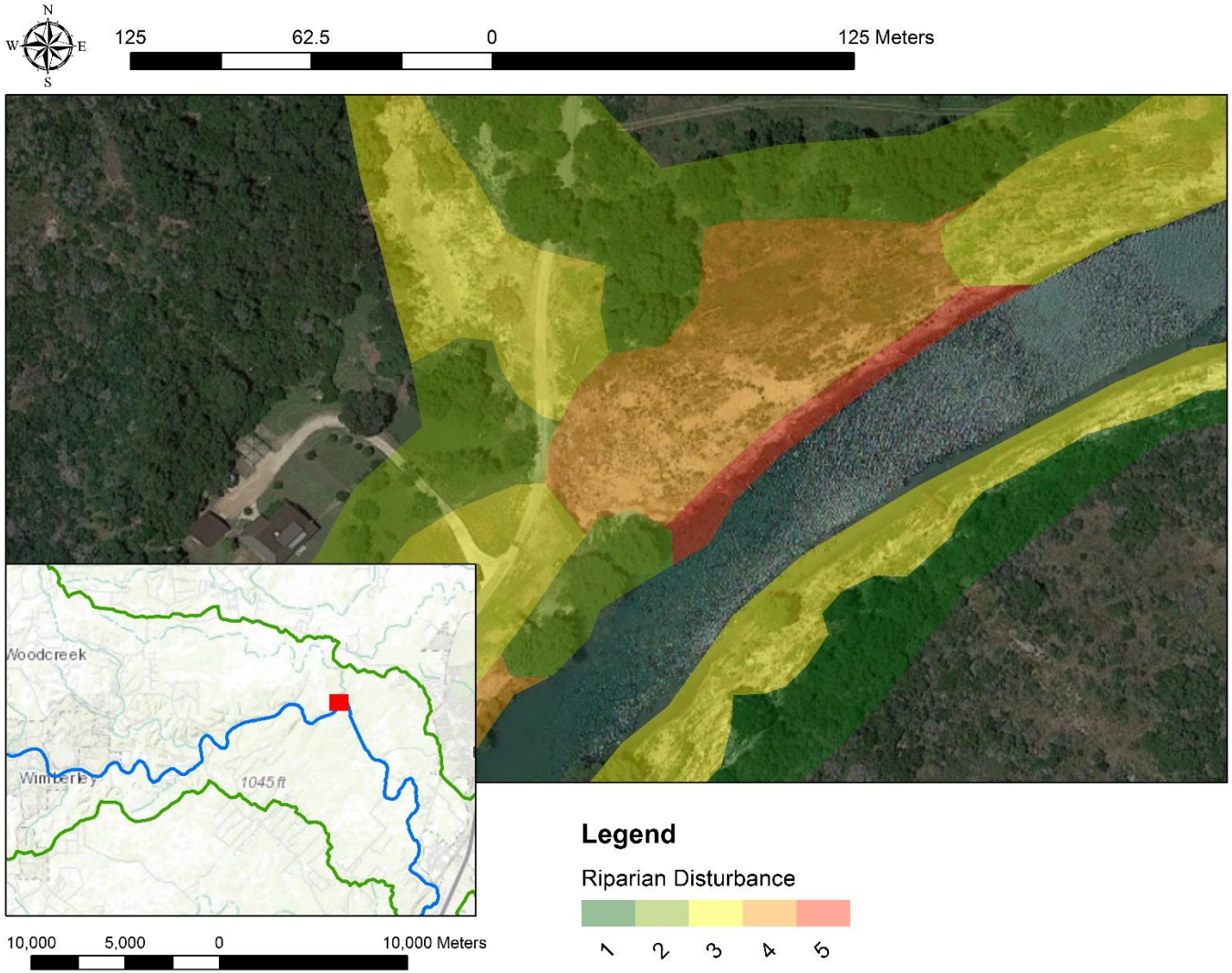

Figure 18 Halifax Creek Confluence. Disturbance mapping at the confluence of Halifax Creek and the Blanco River

f. Disturbance Statistics: Absolute vs Relative

The sampling Python script I wrote provided two outputs for every sample circle. The first output was the total, or absolute, disturbance area separated by category for each sample. The second output was a proportion of the total disturbance per category divided by the total area of all disturbance in the circle. The 'absolute', or total area, outputs were used for tables 12 - 15. A main trend seen in the total area calculations was that all geomorphic and riparian categories correlated moderately to strongly in a positive way with floodway width and negatively with elevation. This means that as the river moves downstream and the floodplain widens, total disturbance area increases for all categories.

The relative disturbance calculations shown in Tables 16 - 19 did not correlate as strongly as the absolute calculations did. They did however give further insight into how the disturbance categories vary with floodway and channel width. For example, while the absolute area relationships with floodway width were all positive, Table 16 (relative area per sample circle) shows that Category 0, Category 4, and Category 5 all have negative relationships with floodway width. This means that, as the floodway widens, the no change category and most severe disturbance categories become less represented in the samples. The opposite is true for the relative relationship with channel width where, as the channel widens, the no change category and most severe riparian and geomorphic disturbance categories become more represented within the sample circles.

Additionally, Category B has a moderately positive correlation with floodway width in both the absolute table (Table 14) and the relative table (Table 18). This means that proportionally, the least severe category of geomorphic disturbance is not represented as much in the upper reaches of the river as in the lower sections. This is possibly due to the

upper reaches being confined, having a smaller floodway, and therefore experiencing more intense disturbance over a smaller area total area. In both the absolute and relative tables, slope and stream power were not well represented and all show low correlation values. This would possibly be different with better measurements derived from field observations.

g. Digitizing and Sampling Caveats

This study was originally conceived from a remote sensing project. The project used 30 meter Landsat 8 imagery pan-sharpened to 15 meters in conjunction with the DigitalGlobe imagery used in this project. Although both the Landsat 8 imagery and the Digital Globe imagery both detected large amounts of disturbance through an NDVI change detection, it was very difficult to detect finer scale phenomena such has individual tree stands to observe their disturbance. Because floodplain stripping occurs at a relatively fine spatial scale, this was problematic.

The advantage of using the Google aerial-imagery was that I could observe the finer scale phenomena. A main disadvantage to using the aerial imagery however was that it was not multispectral and therefore the mapped disturbance data, which could have been generated automatically and with measured precision using remote sensing methods, had to be created manually. Digitizing the disturbance polygons was extremely time-intensive, involved subjectivity. A potential use for this method of manual categorization however would be to use it in conjunction with remote sensing, by identifying large to medium scale phenomenon using coarse grain data, or including a field-validation component. While field work would be preferable in identifying small scale phenomena, it could prove difficult in places that are privately owned making aerial imagery a good

alternative. Another caveat of using the Google imagery is that, because the imagery is hosted by a Web Mapping Tile Service (WTMS), I was unable to change the projection from the Web Mercator Auxiliary Sphere to a more appropriate projection that preserves distance and area instead of shape. Instead, I projected the DigitalGlobe imagery to match the Google imagery for georeferencing which likely affected the accuracy of the area calculations performed throughout the study.

There were also some caveats to the sampling process. Multiple iterations of sampling were performed while developing the process which included variations of the sample shape, size, and spacing. Sample circles with a radius of 80 meters spaced 10 meters apart were decided on because they were able to best capture the most disturbance area along all segments of the study area. The main disadvantage to using 10 meter spacing however is the sample circles overlap at many areas and aren't independent of each other. The overlap affected the statistical outputs because the samples are not mutually exclusive. I attempted to solve this problem in some iterations by creating square and oval buffers that did not overlap each other. However, the square and oval sample buffers could not effectively cover areas along the river with sharp bends and missed disturbance along many sections of the study area. Although the 80-meter sample circles also missed some areas of disturbance most of the missed disturbance was in Category 0, Category 1, Category A, and Category B meaning most of the missed disturbance was either areas of no change or the least severe disturbance which was already the least accurate category in terms of how effectively it can be digitized using visual methods. I also attempted to create sample buffers that grew in size according to

the length of the channel, but that method limited my calculations to proportional areas whereas sample buffers with fixed radius lengths also allowed for a total area calculation.

h. Future Studies

During this study, I found areas that showed signs of disturbance even in the pre-flood imagery. Although both the pre- and post- flood imagery were used for digitizing disturbance, some areas in the pre-flood imagery had trees that had fallen or showed signs of disturbance as a result of a previous flood event. Using Google Earth's historical imagery slider, I was able to identify areas which had been affected by a major flood event on the Blanco River previous to the 2015 Memorial Day floods. A future study could examine disturbance and recovery in the context of both flood events by examining individual features which were disturbed during the first flood and further disturbed during the Memorial Day event. Figures 19 – 22 show the disturbance and recovery over the two flood events, the first taking place in October 2013 and the second being the Memorial Day flood of 2015. Despite aerial imagery being unavailable for part of this study area, the Google imagery project responsible for collecting the data has been collecting imagery for the entire state of Texas since 2011 and they continue to gather the data. For areas that multiple years of imagery has been collected for, this imagery could be used for a variety of studies including studying river evolution and land cover change at a fine scale.

Also, because the Digital Globe imagery are multispectral, a remote sensing analysis could be used to analyze soil and vegetation indices to study disturbance as well as verify the trends seen in this study. Further verification could be achieved by using the GIS products from this study to identify specific areas to perform field work. The layers

would also be useful in identifying areas to install new stream gauges. The massive disturbance which this flood caused warrants further monitoring and hazard mitigation efforts in the future. Finally, due to the lack of accurate discharge data, a hydrologic and hydraulic modeling study would benefit this project immensely. The modeling could be used to replicate the flood and further examine the tributary confluences, dams, and other areas in the study area. In addition to the hydrologic analysis bed material load, bed material size, and bank material could be examined in the same areas using field methods.

Figure 19 The Blanco River Pre-October Flood. A section of the Blanco River before the October 2013 flood event.

Figure 20 The Blanco River Post-October Flood. A section of the Blanco River after the October 2013 flood event.

Figure 21 The Blanco River Pre-Memorial Day Flood. A section of the Blanco River which has recovered from the 2013 flood event. Captured before the 2015 Memorial Day flood event.

Figure 22 The Blanco River Post-Memorial Day Flood. A section of the Blanco River after the 2015 Memorial Day flood event. Similar disturbance patterns are seen with the 2015 flood as were seen with the 2013 flood.

VI. CONCLUSION

This study shows that high resolution satellite and aerial imagery can be used to map, categorize, and quantify riparian and geomorphic disturbance caused by catastrophic flooding on the Blanco River. Pre- and post- flood imagery make it possible to identify areas of floodplain stripping as well as other fine scale disturbance phenomena along the river. By mapping and categorizing geomorphic disturbance and comparing the GIS product to existing FEMA floodplain layers, I have shown that there is a relationship between total disturbance area and the width of the FEMA floodway as well as a relationship between the relative disturbance area and floodway width. Similar relationships were identified between disturbance and channel width; however, no relationships were found with stream power possibly due to inaccuracies in the calculations. I identified a gradient of decreasing disturbance moving away from the channel by using floodplain layers as a proxy for distance and examining the relationships between areas per disturbance category. I created a custom statistical sampling method to further examine relationships between disturbance categories and river properties. Digitization and categorization accuracy were verified by intersecting geomorphic and riparian disturbance categories and comparing relationships between total disturbance and relative disturbance values. Patterns of biogeomorphic disturbance mentioned in previous literature such as across meander scour and parallel chute scour were identified as well as patterns of severe disturbance at tributary confluences. Finally, the advantages and disadvantages of using high-resolution imagery to manually categorize flood disturbance were discussed as well as techniques which could be used to improve these existing methods as well as expand on them in future studies.

APPENDIX SECTION

APPENDIX A - PANSHARPENING SCRIPT

```
import arcpy
import glob
import os
workspace = r"E:\Thesis\DIGITALGLOBE"
arcpy.env.workspace = workspace
arcpy.env.overwriteOutput = True
out_path = r"G:\OutTIF"
MUL_TIF_files =
r"E:\Thesis\DIGITALGLOBE\055084837010_01\055084837010_01_P002_MUL"
PAN_TIF_files =
r"E:\Thesis\DIGITALGLOBE\055084837010_01\055084837010_01_P002_PAN"
MUL_tifCounter = len(glob.glob1(MUL_TIF_files,"*.tif"))
MUL_list = []
for root, dirs, files in os.walk(MUL_TIF_files):
    for file in files:
        if file.endswith(".TIF"):
            MUL_file = os.path.join(root, file)
            MUL_list.append(MUL_file)
print str(MUL_tifCounter) + " Multispectral Files"
PAN_tifCounter = len(glob.glob1(MUL_TIF_files,"*.tif"))
PAN_list = []
for root, dirs, files in os.walk(PAN_TIF_files):
    for file in files:
        if file.endswith(".TIF"):
            PAN_file = os.path.join(root, file)
            PAN_list.append(PAN_file)
print str(PAN_tifCounter) + " Panchromatic Files"
for Mpath,Ppath in zip(MUL_list,PAN_list):
    print Mpath
    print Ppath
    Mfile = os.path.split(Mpath)[1]
    Pfile = os.path.split(Ppath)[1]
    Msplit = os.path.splitext(Mfile)[0]
    Mout = Msplit + ".TIF"
    print Mout
    in_raster = Mpath
    red_channel = 5
    green_channel = 3
    blue_channel = 2
    infrared_channel = 7
    out_raster_dataset = os.path.join(out_path,Mout)
    print out_raster_dataset
```

```
    in_panchromatic_image = Ppath
    pansharpening_type = "IHS"
    sensor = "WorldView-2"
    band_indexes = "5 3 2 7"
    out_pan_weight = arcpy.ComputePansharpenWeights_management (in_raster,
in_panchromatic_image, band_indexes)
    pansharpen_weights = out_pan_weight.getOutput(0)
    print pansharpen_weights
    pansplit = pansharpen_weights.split(";")
    red_weight = pansplit[0].split(" ")[1]
    green_weight = pansplit[1].split(" ")[1]
    blue_weight = pansplit[2].split(" ")[1]
    infrared_weight = pansplit[3].split(" ")[1]
    print "Pansharpening..."
    arcpy.CreatePansharpenedRasterDataset_management (in_raster, red_channel,
green_channel, blue_channel,\
    "",out_raster_dataset,in_panchromatic_image,
pansharpening_type,red_weight,green_weight,blue_weight,"")
```

APPENDIX B – CLIP AND CALCULATE SCRIPT (SAMPLE CIRCLES)

```
import arcpy
import os
workspace = r"E:\Thesis\_SampleCircles\Round17"
arcpy.env.workspace = workspace
arcpy.env.overwriteOutput = True
if not os.path.exists(workspace):
   os.makedirs(workspace)
riparianDist = r"E:\Thesis\DIGITIZING\Backup\RiparianDisturbance.shp"
geomorphicDist = r"E:\Thesis\DIGITIZING\Backup\GeomorphicDisturbance.shp"
sampleCircles = r"E:\Thesis\_SampleCircles\round12\160mSampcircles.shp"
disturbanceLayer = riparianDist
ripoutTableName = "ripstat.dbf"
geooutTableName = "geostat.dbf"
if disturbanceLayer == riparianDist:
   outTableName = ripoutTableName
elif disturbanceLayer == geomorphicDist:
   outTableName = geooutTableName
else:
   quit()
field_names = ['ORIG_FID']
#create empty feature class
arcpy.CreateFeatureclass_management (workspace, "MasterCircles.shp", "POLYGON",
sampleCircles)
masterCircles = os.path.join(workspace,"MasterCircles.shp")
sCursor = arcpy.da.SearchCursor(sampleCircles, field_names)
mainGroupstr = outTableName
mainGroupTable = os.path.join(workspace,mainGroupstr)
counter = 0
#Check if area field exists and add if not
lstFields = arcpy.ListFields(disturbanceLayer)
x = False
for field in lstFields:
   if field.name == "area":
      print "Field exists"
      x = True
if x <> True:
   print "area Field does not exist"
   print "Adding area field..."
   arcpy.AddField_management(disturbanceLayer, "area", "DOUBLE")
for row in sCursor:
   clipNum = "clip" + str(row[0]) ##+ ".shp"
   where_clause = '"ORIG_FID" = ' + "%s"%(row[0])
   preclipNum = "preclip" + str(row[0])
   preclipLayer = os.path.join(workspace,preclipNum)
   pre_out_clip_str = "preclip" + str(row[0]) + ".shp"
```

```
pre_temp_out_clip = os.path.join(workspace,pre_out_clip_str)
arcpy.MakeFeatureLayer_management (sampleCircles,preclipLayer,where_clause)
print clipNum
out_clip_str = "clip" + str(row[0]) + ".shp"
temp_out_clip = os.path.join(workspace,out_clip_str)
print "Clipping item " + str(out_clip_str)
arcpy.Clip_analysis(disturbanceLayer, preclipLayer, pre_temp_out_clip)
arcpy.Clip_analysis(pre_temp_out_clip, disturbanceLayer, temp_out_clip)
sumOutstr = "sumstats" + str(row[0]) + ".dbf"
sumOutFolder = os.path.join(workspace,"sumstats")
if not os.path.exists(sumOutFolder):
   os.makedirs(sumOutFolder)
sumOut = os.path.join(sumOutFolder,sumOutstr)
tempPgs = temp_out_clip
geometry = arcpy.CopyFeatures_management(temp_out_clip,arcpy.Geometry())
totGeom = 0
for g in geometry:
   partGeom = g.getArea("PLANAR","SQUAREMETERS")
   totGeom = totGeom + partGeom
print totGeom
print "Calculating Area..."
exp = "!SHAPE.AREA@SQUAREMETERS!"
arcpy.CalculateField_management(tempPgs, "Area", exp, "PYTHON_9.3")
print "Calculating stats..."
arcpy.Statistics_analysis (temp_out_clip, sumOut, [["Area","SUM"]], "Disturbanc")
print "Calculating CircleIDs..."
arcpy.AddField_management(sumOut, "CircleID", "LONG")
exp2 = "%s"%int(row[0])
arcpy.CalculateField_management(sumOut, "CircleID", exp2, "PYTHON_9.3")
arcpy.AddField_management(sumOut, "PropArea", "DOUBLE")
exp3 = "!SUM_Area!/%s"%(totGeom)
arcpy.CalculateField_management(sumOut, "PropArea", exp3, "PYTHON_9.3")
if counter == 0:
   print "Creating base table..."
   arcpy.CreateTable_management (workspace, mainGroupstr,sumOut)
else:
   pass
print "Appending..."
arcpy.Append_management (sumOut,mainGroupTable)
print "Deleting temp layers..."
arcpy.Delete_management(temp_out_clip)
arcpy.Delete_management(sumOut)
arcpy.Delete_management (preclipLayer)
arcpy.Delete_management (pre_temp_out_clip)
counter =+ 5
```

LITERATURE CITED

Anderson, B. G., Rutherfurd, I. D., and Western, A. W. 2005. An analysis of the influence of riparian vegetation on the propagation of flood waves. Environmental Modeling & Software 21:1290–1296.

Abernethy, B., and Rutherfurd, I. D. 2001. The distribution and strength of riparian tree roots in relation to riverbank reinforcement. Hydrological Processes 15 (1):63–79.

Aguiar, F. C. C. A., Martins, M. J., Silva, P. C., and Fernandes, M. R. 2016. Riverscapes downstream of hydropower dams: Effects of altered flows and historical land-use change. Landscape and Urban Planning 153:83–98.

Bagnold, R. A. 1966. An Approach to the Sediment Transport Problem from General Physics. By R. A. Bagnold. U.S. Geological Survey Professional Paper 422-I, pp. v 37, with 15 figs, and 1 table. U.S. Government Printing Office, Washington, D.C., 1966. Price 35 cents. Geological Magazine 104 (04):409.

Baker, V. R. 1977. Stream-channel response to floods, with examples from central Texas. Geological Society of America Bulletin 88 (8):1057.

Beard, L. R. 1975. Generalized evaluation of flash-flood potential. Texas Univ. Center Research Water Resources Tech. Rept. CRWR-124.

Bourke, M. C. 1994. Cyclical construction and destruction of flood dominated flood plains in semiarid Australia. Variability in Stream Erosion and Sediment Transport (Proceedings of the Canberra Symposium) 224.

Broad, I. 2014. Create Points on Lines. arcgis.com. https://www.arcgis.com/home/item.html?id=13c92d8877054b979ac2f69547bd50f1 (last accessed 1 December 2016).

Caskey, S. T., Blaschak, T. S., Wohl, E., Schnackenberg, E, Merritt, D. M., and Dwire. K.A. 2014. Downstream effects of stream flow diversion on channel characteristics and riparian vegetation in the Colorado Rocky Mountains, USA. Earth Surface Processes and Landforms 40 (5):586–598.

Dean, D. J., and Schmidt, J. C. 2011. The role of feedback mechanisms in historic channel changes of the lower Rio Grande in the Big Bend region. Geomorphology 126 (3-4):333–349.

Dobie, D. R. 1948. A Brief History of Hays County and San Marcos Texas. The San Marcos Record.

Forman, R. T. T., and Godron, M. 1981. Patches and Structural Components For A Landscape Ecology. Bioscience 31:2369–2379.

GBRA. 2013. Blanco River Watershed: River Segments, Descriptions and Concerns. Guadalupe-Blanco River Authority. http://www.gbra.org/documents/publications/basinsummary/2013e.pdf (last accessed 22 March 2017).

Graf, W. L. 2006. Downstream hydrologic and geomorphic effects of large dams on American rivers. Geomorphology 79 (3-4):336–360.

Griffith, G. E., Bryce, S. B., Omernik, J. M., and Rogers, A. 2008. Ecoregions of Texas. Texas Commission on Environmental Quality. https://archive.epa.gov/wed/ecoregions/web/html/tx_eco.html (last accessed 14 March 2016).

Guillén-Ludeña, S., M. Franca, A. Cardoso, and A. Schleiss. 2016. Evolution of the hydromorphodynamics of mountain river confluences for varying discharge ratios and junction angles. Geomorphology 255:1–15.

Hupp, C. R. 1992. Riparian Vegetation Recovery Patterns Following Stream Channelization: A Geomorphic Perspective. Ecology 73 (4):1209–1226.

Indriasari, V. 2015. Linear Sampling Toolbox. arcgis.com. https://www.arcgis.com/home/item.html?id=d16ec9f1a16b4e0caca7b2398bff941b (last accessed 1 December 2016).

IPCC, 2014: Climate Change 2014: Synthesis Report. Contribution of Working Groups I, II and III to the Fifth Assessment Report of the Intergovernmental Panel on Climate Change [Core Writing Team, R.K. Pachauri and L.A. Meyer (eds.)]. IPCC, Geneva, Switzerland, 151 pp.

Julian, J. P., Podolak, C. J. P., Meitzen, K. M., Doyle, M. W., Manners, R. B., Hester, E. T., Ensign, S., Wilgruber, N. A. 2016. Shaping the Physical Template: Biological, Hydrological, and Geomorphic Connections in Stream Channels In Stream Ecosystems in a Changing Environment, ed. Jones, J. B. and Stanley, E. H., 85-133. Amsterdam: Elsevier Academic Press.

Meitzen, K. M. 2005. Overbank Flooding and Sedimentation Patterns in a Floodplain Environment, Lower Guadalupe River, Texas. University of Texas Undergraduate Research Journal 4(1): 34 – 47.

Nanson, G. C. 1986. Episodes of vertical accretion and catastrophic stripping: A model of disequilibrium flood-plain development. Geological Society of America Bulletin 97 (12):1467.

Nanson, G., and Croke, J. 1992. A genetic classification of floodplains. Geomorphology 4 (6):459–486.

Nanson, G. C., and Young, R. W. 1981. Overbank deposition and floodplain formation on small coastal streams of New South Wales. Zeitschrift fur Geomorphologie 25:332–347.

NRCS Web Soil Survey. United States Department of Agriculture - Natural Resources Conservation Service. https://websoilsurvey.sc.egov.usda.gov/App/HomePage.htm (last accessed 26 March 2017).

Owen, A. (2015). Statistics support for students. Correlation. http://www.statstutor.ac.uk/ (last accessed 3/17/2017).

Patton, P. C., and Baker, V. R. Geomorphic response of central Texas stream channels to catastrophic rainfall and runoff. Geomorphology in arid regions: 8th annual geomorphology symposium, Binghamton, Sept. 1977, proceedings. ed. Doehring, D. O. 1977. Binghamton: Publications in Geomorphology.

Sansom, A., Xia, Y., Clary, M., Parchman, L., Blount, M., and Warren, E. 2010. Blanco - San Marcos Watershed Modeling: Land Use & Land Cover Change and Its Impact on Streamflow and Non -Point Source Pollution.

Simon, A., and Collison, A. J. C. 2002. Quantifying the mechanical and hydrologic effects of riparian vegetation on streambank stability. Earth Surface Processes and Landforms 27 (5):527–546.

Schumm, S. A. 1963. A tentative classification of alluvial river channels. Washington, D.C.: U.S. Geological Survey.

Schumm, S. A. 1968. River adjustment to altered hydrologic regimen, Murrumbidgee River and paleochannels, Australia. Washington: U.S. Govt. Print. Off.

Smith, B. A., Hunt, B. B., Andrews, A. G., Watson, J. A., Gary, M. O., Wierman, D. A., and Broun, A. S. 2015. Surface water–groundwater interactions along the Blanco River of central Texas, USA. Environmental Earth Sciences 74 (12):7633–7642.

TWDB. 2017. Geologic Atlas of Texas 1:250,000 Scanned Map Sheets. Texas Water Development Board. https://www.twdb.texas.gov/groundwater/aquifer/GAT/ (last accessed 26 March 2017).

Warner, R. F. 1997. Floodplain stripping: another form of adjustment to secular hydrologic regime change in Southeast Australia. Catena 30 (4):263–282.

Wolman, M. G., and Leopold, L. B. 1965. River flood plains: some observations on their formation: physiographic and hydraulic studies of rivers. Washington, D.C.: United States Government Printing Office.

Wolman, M. G., and Miller, J. P. 1960. Magnitude and Frequency of Forces in Geomorphic Processes. The Journal of Geology 68 (1):54–74.